TAMPEREEN TEKNILLINEN YLIOPISTO
TAMPERE UNIVERSITY OF TECHNOLOGY

MARIA NIZNIK

# ANALYSIS OF ENHANCED LIGHT HARVESTING AND QUANTUM EFFICIENCY IN TEXTURED SILICON SOLAR CELLS

Master of Science Thesis

Examiners: Professor Helge Lemmetyinen
Professor Risto Raiko
Examiners and topic approved by the Faculty Council of the Faculty of Natural Sciences on 4 September 2013

# ABSTRACT

TAMPERE UNIVERSITY OF TECHNOLOGY
Master's Degree Programme in Environmental and Energy Technology
NIZNIK, MARIA: Analysis of Enhanced Light Harvesting and Quantum Efficiency in Textured Silicon Solar Cells
Master of Science Thesis, 67 pages, 6 Appendix pages
October 2013
Major: Power Plant and Combustion Technology
Examiner: Professor Helge Lemmetyinen, Professor Risto Raiko
Keywords: Texturing, quantum efficiency, reflection, transmittance, solar cell, pyramids

Textures on semiconductor materials, such as monocrystalline and multicrystalline silicon (Si), consist of an array of geometrical structures. The main advantage of such structures is the fact that they are able to significantly increase the amount of transmitted light on the cell surface without the use of other antireflection and light trapping techniques, such as antireflection coatings. Texturing a Si wafer includes three benefits: decrease in external reflection, increase in internal reflection preventing the rays from escaping the solar cell, and increase in effective absorption length due to tilted rays.

The aim of the thesis is to determine the influence of textures on the total quantum efficiency (QE) of the cell. Firstly, various types of texture structures with different physical parameters, as well as their antireflection and light trapping capabilities are investigated. It becomes evident throughout a brief literature review of textures that regular inverted pyramids are featured in the most efficient commercial solar cell and provide the best optical enhancements. State-of-the-art modeling techniques that aim at developing light simulation programs targeted to analyze solar cells' reflectance were also investigated. A simulation code based on a chosen analytical geometrical model type is developed and employed to estimate front-face reflection and transmittance of regular upright pyramids in 2D. It is noted, that the results of surface reflection obtained by the simulation code are fairly consistent with the results found in the literature, signifying that such complex problem does not necessarily require a numerical approach. Finally, the internal quantum efficiency (IQE) and external quantum efficiency (EQE) analyses of textured and perfectly flat cells are performed and the obtained results are compared to each other.

The simulations show that texturing does indeed provide significant decrease in front-face reflection in comparison with a flat Si surface and a single-layer antireflection coating with an optimal thickness. Furthermore, throughout the study it becomes clear that surface recombination velocity does not affect the IQE significantly in thick solar cells. Therefore, the deteriorating effect on the cell's electrical performance, an increase in surface recombination velocity due to an increased front surface area in textured cells, is ignored. Also, it is noticed that increased front surface recombination velocity affects only a small fraction of wavelengths of interest, and the surface of a cell can be also passivated to prevent surface recombination altogether. The IQE analysis also reveals that textured cells provide higher IQE values in the longer wavelength region than flat cells, due to tilted light path.

The results obtained in this thesis highlighted the numerous benefits of texturing silicon solar cells, since more light is able to penetrate the surface and contribute to the short circuit current.

# TIIVISTELMÄ

TAMPEREEN TEKNILLINEN YLIOPISTO
Ympäristö- ja energiatekniikan koulutusohjelma
NIZNIK, MARIA: Parannetun valokeruun ja kvanttihyötysuhteen analyysi teksturoiduissa piiaurinkokennoissa
Diplomityö, 67 sivua, 6 liitesivua
Lokakuu 2013
Pääaine: Voimalaitos- ja polttotekniikka
Tarkastaja: professori Helge Lemmetyinen, professori Risto Raiko
Avainsanat: Teksturointi, kvanttihyötysuhde, heijastus, läpäisysuhde, aurinkokennot, pyramidit

Puolijohde materiaalina käytetään yleensä yksi- tai monikiteistä piitä. Näiden materiaalien pinnoille voidaan etsata rakenteeltaan erityyppisiä ja -kokoisia pintarakenteita. Tällaista prosessia kutsutaan teksturoinniksi. Teksturoinnin avulla voidaan nostaa läpäisseen valon määrää merkittävästi käyttämättä muita valon heijastuksenesto ja kaappaus menetelmiä, kuten heijastuksenestopinnoitetta. Piipuolijohteiden teksturoinnilla alennetaan materiaalin optisia häviöitä kolmella eri tavalla: etupinnan heijastusta pienenentämällä, estämällä sisäisesti heijastuvien fotonien poistuminen kaappaamalla ne, sekä pidentämällä valon absorptiomatkaa ohjaamalla fotonit kulkemaan viistosti pintarakenteiden läpi.

Tämän työn tavoite on tutkia miten pintarakenteet vaikuttavat piiaurinkokennojen heijastukseen sekä kvanttihyötysuhteeseen. Aluksi, työssä tutkitaan erityyppisiä pintarakenteita ja niiden fyysisiä parametreja, sekä rakenteiden kykyä parantaa kennon optisia ominaisuuksia. Kirjallisuusselvityksessä tulee ilmi, että säännöllisiä käänteisiä pyramideja käytetään korkeahyötysuhteisissa aurinkokennoissa, sillä ne parantavat eniten piin optisia ominaisuuksia. Pintarakenteiden mallintamiskeinoja kehitetään koko ajan ja tavoitteena on mm. analysoida kennojen heijastavuutta. Työssä kehitetään simulaatiokoodia, joka perustuu valittuun analyyttiseen geometriseen malliin (2D:ssa) ja sitä käytetään arvioitaessa aurinkokennon etupinnan heijastusta ja läpäisysuhdetta säännöllisissä pystypyramidi -rakenteissa. Simuloinnin tuloksia verrataan muiden tutkijoiden saamiin tuloksiin. Tulokset ovat keskenään yhdenmukaisia, mikä viittaa siihen, että tämäntyyppinen monimutkainen ongelma ei välttämättä vaadi numeerista lähestymistapaa. Lopuksi, arvioidaan teksturoidun ja tasaisen kennonpinnan sisäisiä ja ulkoisia kvanttihyötysuhteita sekä verrataan näitä keskenään.

Simuloinnin tulokset osoittivat, että teksturointi heikentää merkittävästi etupinnan heijastavuutta verrattuna tasaiseen pintaan tai yksikerroksiseen heijastuksenestopinnoitteeseen, jolla on optimaalinen paksuus. Lisäksi tutkimuksessa selviää, että pintarekombinaationopeus ei vaikuta paksuissa kennoissa olennaisesti sisäiseen kvanttihyötysuhteeseen. Tämän takia teksturoitujen kennojen taipumus heikentää kennojen sähköistä toimintaa, johtuen pintarekombinaationopeuden kasvusta, kasvaneen etupinnan pinta-alan vuoksi, jätettiin huomiotta. Huomattiin myös, että etupintarekombinaationopeus vaikuttaa vain pieneen osaan tarkastetusta aallonpituusalueesta. Tarvittaessa kennon etupintaa on myös mahdollista passivoida välttääkseen etupintarekombinaatiota kokonaan. Kvanttihyötysuhteen analyysi osoitti, että sisäisen kvanttihyötysuhteen arvot pitkillä aallonpituuksilla ovat suuremmat teksturoiduilla kuin tasaisilla kennoilla kallistetun valonpolun ansiosta.

Työssä saadut tulokset korostavat teksturoinnin lukuisia etuja, sillä enemmän valoa läpäisee piimateriaalin pinnan ja parantaa kennon oikosulkuvirtaa.

# PREFACE

This Master of Science Thesis was done in the Department of Environmental and Energy Engineering in Tampere University of Technology. The thesis is based on the three-month internship that I did in TUT's partner university in France, Institut National des Sciences Apliquées de Lyon (INSA de Lyon), in cooperation with Centre de Thermique de Lyon (CETHIL).

I would like to express my gratitude to Prof. Helge Lemmetyinen. His excellent knowledge and extensive experience on the topic of photovoltaic cells provided me with valuable and expert feedback, and gave me confidence in my research. Furthermore, I would like to thank Prof. Risto Raiko for his encouragement, advice and guidance.

I would also like thank my parents, Rosetta and Tapio Lehtonen, who stand by me in all my life endeavors and are the best role models and most supporting and loving parents one can have.

Finally, I want to thank Raphaël Goossens for his support, participation and patience.

Tampere 14.9.2013

Maria Niznik

# TABLE OF CONTENTS

# LIST OF SYMBOLS AND ABBREVIATIONS

## Symbols

| | |
|---|---|
| A | Light path that involves two bounces |
| $abs$ | Absorber region of the cell |
| B | Light path that involves three bounces |
| $b$ | Base region of a solar cell |
| $bs$ | Back surface of a solar cell |
| $c$ | Speed of light in vacuum |
| $E$ | Electric field |
| $e$ | Emitter region of a solar cell |
| $E_c$ | Conduction band energy |
| $E_g$ | Semiconductor band gap |
| $E_{ph}$ | Photon energy |
| $E_v$ | Valence band energy |
| $f$ | Frequency of light wave |
| $f_A$ | Probability coefficient of light following path A |
| $f_B$ | Probability coefficient of light following path B |
| $g$ | Expression in global coordinates |
| $H$ | Thickness of a solar cell |
| $h$ | Planck's constant |
| $I$ | Solar flux |
| $i$ | Path A or path B |
| $I_0$ | Incident solar flux |
| $I_{R,reg,up}$ | Total reflected flux from upright pyramids |
| $I_{T,reg,up}$ | Total transmitted flux from upright pyramids |
| $j$ | Pyramid facet |
| $J_L$ | Light-generated current |
| $J_{sc}$ | Short-circuit current |
| $k$ | Extinction index of a wave in a medium |
| $L$ | Diffusion length of minority carriers |
| $m$ | Total number of bounces of a certain light path |
| $n$ | Refractive index |
| $\bar{n}$ | Complex refractive index |
| $\hat{p}$ | Parallel polarization |

| | |
|---|---|
| $r$ | Reflection coefficient |
| $S$ | Recombination velocity |
| $\hat{s}$ | Perpendicular polarization |
| $scr$ | Space charge region of a solar cell |
| $t$ | Transmittance |
| $V_{oc}$ | Open-circuit voltage |
| $v$ | The speed of light in a material |
| $w$ | Thickness of a solar cell region |
| $\alpha$ | Absorption coefficient |
| $\varepsilon$ | Electrical permittivity |
| $\theta$ | Angle of incident light |
| $\lambda$ | Wavelength of light |
| $\mu$ | Magnetic permeability |
| $\rho$ | Reflectance |
| $\varphi$ | Polarization angle |

## Abbreviations

| | |
|---|---|
| AM | Air mass |
| AM1.5 | Air mass 1.5 |
| AM1.5g | Air mass 1.5 global |
| ARC | Antireflection coating |
| BAFT | Back face textured |
| BEM | Boundary element method |
| BOFT | Both faces textured |
| c-Si | Monocrystalline silicon |
| EHP | Electron-hole pair |
| EQE | External quantum efficiency |
| FEM | Finite element method |
| FFT | Front face textured |
| FTDM | Finite time domain method |
| IQE | Internal quantum efficiency |
| IR | Infrared |
| KOH | Potassium hydroxide |
| mc-Si | Multicrystalline silicon |
| NaOH | Sodium hydroxide |
| PERL | Passivated emitter rear locally diffused |
| PV | Photovoltaic |

| | |
|---|---|
| QE | Quantum efficiency |
| RIE | Reactive-ion etching |
| SR | Spectral response |
| Si | Silicon |
| SRH | Shockley-Read-Hall |
| wt% | Weight percent |
| 1D | One-dimensional |
| 2D | Two-dimensional |
| 3D | Three-dimensional |

# 1 INTRODUCTION

General concern about climate change and increase of carbon dioxide emissions empowered by a continuous increase in energy consumption has raised interest in sustainable energy sources, such as photovoltaic systems (PV). Photovoltaic solar cells are able to convert energy from the incident photons into the creation of mobile charge carriers that finally contribute to the output current of such devices. (Green, 1987) Silicon is the most common semiconductor material used in terrestrial photovoltaic cells. The theoretical efficiency of a monocrystalline silicon (c-Si) photovoltaic cell can approach 29 %, while the world record for the best silicon solar cell is 24.3 %. However, industrial c-Si solar cells typically have an efficiency of 17 %. (Fraas & Partain, 2010)

Many factors contribute to limit the PV cell efficiency, such as limitations based on the fundamental properties of silicon semiconductors. Optical losses are one of the most important issues that limit the conversion of incident solar energy into current. The amount of current produced by the solar cell (short-circuit current) is dependent on the fraction of light that is absorbed by the silicon solar cell and converted without losses into electric energy. (Tiedje et al., 1984) Nevertheless, due to high refractive index values crystalline semiconductor materials poorly absorb the incident light. About 30-40 % of incident light is lost due to reflection on the front-surface of the cell. (Poruba, et al., 2000; Miles et al., 2005)

Surface textures are one of the most efficient ways to solve the problem of high reflection of semiconductor materials. Various texture structures, such as random and inverted pyramids can be created using, for instance wet chemical etching techniques on monocrystalline silicon solar cells. These surfaces can achieve light scattering (or diffuse reflection) from the surface of the solar cell through multiple reflections (Miles et al., 2005). Surface textures can also increase the absorption of light through trapping poorly absorbed light within the cell and increasing absorption lengths. (Fraas & Partain, 2010; Miles et al., 2005)

Surface textures can be used in combination with an antireflection dielectric coating. It has been shown that surface textures on their own can decrease reflection to approximately 10 % and together with an antireflection coating (ARC) light reflection is further decreased to below 4 % (Baker-Finch & McIntosh, 2010). In order, to determine the beneficial effects of surface textures on incident light harvesting, comprehensive light trapping simulation programs, such as ray tracing simulations, were created. These programs perform an analysis of light behavior on various textures with different parameters, such as texture size. (Byun et al., 2011) However, most of these methods are computationally intense (Baker-Finch & McIntosh, 2010). It was also noticed that a

great deal of reflection studies were performed in such way that the reflection of an already textured c-Si solar cell was simply measured. This approach naturally provides little room for optimization of texturing. Due to these reasons, a simplified analytical model was chosen in this thesis to simulate textured surfaces (regular upright pyramids).

In order to characterize the solar cell performance, quantum efficiency (QE) of solar cells can be investigated. Quantum efficiency indicates the fraction of incident photons at different wavelengths on a PV cell that are capable of contributing to the external photocurrent. Internal quantum efficiency considers only the photons that were not lost by reflection. It thus provides a more accurate analysis and highlights the importance of cell's reflection on the overall device performance.

Quantum efficiency analysis is capable of taking into account other important parameters that govern the solar cell performance, such as recombination. Recombination is the process that is opposite of generation and thus is detrimental to the solar cell performance. Photon-generated electrical charges that contribute to the short-circuit current of the solar cell can recombine in the bulk of the semiconductor and on the solar cells front and rear surfaces. Front-surface recombination happens due to the defects on the surface provoked by the abrupt silicon crystal edge breakdown. Recombination on the cell surface is thus particularly important in textured silicon surfaces since texturing results in increased front surface area. Therefore, textured silicon solar cells have an increased surface recombination rate in comparison with flat cells. (Yang et al., 2008; Markvart & Castaner, 2004; Gjessing, 2012)

To sum up, while textured surfaces are able to improve solar cell performance by increasing photon absorption, they can also increase recombination in the cell, which on the other hand negatively affects the conversion efficiency of the device. Therefore, the influences of texturing must be investigated through QE analysis. Texturing parameters and configuration can thus be optimized to extract maximum benefit in terms of conversion efficiency.

## 1.1 Thesis overview

The aim of this thesis was to investigate, which surface textures are available for the state-of-the-art silicon solar cells and how these surfaces influence the front-surface reflection. In order to calculate the front-surface reflection a literature review on the existing modeling approaches was performed and an appropriate model was chosen. The analysis is extended to investigating how decreased reflection influences the overall performance of silicon solar cells through a quantum efficiency analysis.

In the first part of the thesis an overview of solar cell physics is presented in order to help the reader understand in more depth the factors that contribute to limiting the conversion efficiency of the solar cell. This chapter also highlights the importance of optical losses on the quantum efficiency and the overall performance of the solar cell. In Chapter 2 the main principles of geometric optics are also highlighted since they are relevant to the method chosen to analyze reflection of textured surfaces. Chapter 3 deals

with different methods of texturing crystalline silicon solar cells with distinct crystallographic orientations. Different surface textures and their parameters are investigated, as well. Also, the means through which textured surfaces achieve decreased reflection and their impact on the solar cell performance are explained in this chapter. Chapter 4 briefly presents various approaches that simulate light behavior on complex surface structures and limitations of these models. The chosen analytical method to model solar cell texturing is presented. Equations that govern the IQE of a textured and flat cell are presented, with the associated simplifications. In Chapter 5 the results of reflectance and transmittance of regular upright pyramids are presented. The obtained values of reflection are compared with reflection values of textured silicon solar cells found in literature. The results are also compared with the calculated reflection values of a bare silicon surface and of a silicon dioxide ($SiO_2$) single layer antireflection coating on a silicon substrate. In addition, in this chapter the results of IQE and EQE values of a textured and flat solar cell are shown. Discussion of the obtained results and ideas for future development conclude Chapter 5. Finally, conclusions are drawn on the applicability and reliability of the reflection analysis results based on the chosen model. Also, the overall influence of textured surfaces on silicon solar cell performance is discussed.

# 2 THEORETICAL BACKGROUND

## 2.1 Introduction

This chapter outlines the background knowledge that was required for the completion of this thesis. Section 2.2 introduces a quick overview of crystalline silicon solar cells. Section 2.3 presents the operating principles of solar cells in general, highlighting the most important concepts that help understand how electricity is generated from the sun radiation and which factors limit the performance efficiency of photovoltaic cells. The main factors provoking optical losses are discussed in Section 2.4. Finally, the effects of optical and recombination losses on PV cell performance are investigated in Section 2.5 with the help of such concepts as quantum efficiency and spectral response.

## 2.2 An overview of Si solar cells

A semiconductor junction device converts directly incident light into electricity. This phenomenon is otherwise known as the photovoltaic effect and was first observed by Becquerel in 1839 (Miles et al., 2005; Dell & Rand, 2004). The first photovoltaic power generating c-Si solar cell was developed almost over 60 years ago with conversion efficiency of only 6 %. (Markvart & Castaner, 2004)

Silicon is one of the most abundant elements in the earth's crust and it is an elemental semiconductor having a band gap that is nearly a perfect match to the solar spectrum. These factors make it one the most commonly used materials for photovoltaic solar devices. (Tiedje et al., 1984) Other advantages of using silicon as solar cell material include its mature processing technology and non-toxicity, which is of particular importance from the environmental point of view (Möller et al., 2005). For these reasons the majority of all commercial photovoltaic cells are fabricated from crystalline silicon. Also, significant improvements have been made in the solar cell technology and c-Si solar cell efficiencies are reaching up to 25 % (Green et al., 2012; Dell & Rand, 2004) as seen in Figure 2.1.

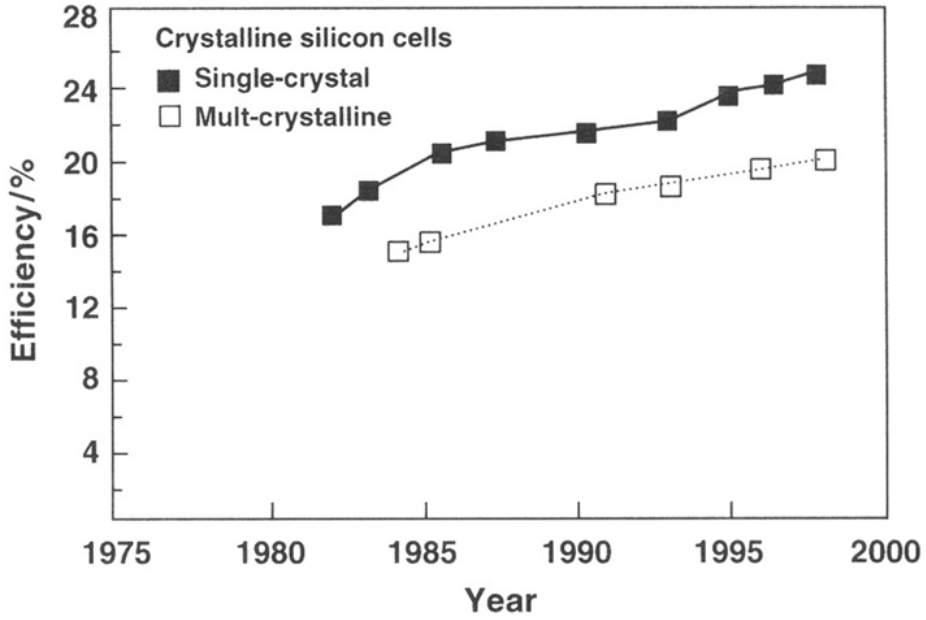


***Figure 2.1.*** *The evolution of monocrystalline and multicrystalline silicon solar cell efficiencies (Dell & Rand, 2004).*

Improvements in optical and electrical designs of the cells played a crucial role in enhancing the conversion efficiencies of photovoltaic cells (Dell & Rand, 2004). Optical improvements have been achieved namely by reducing front-surface reflection and improving light-trapping within the cell (see Chapter 3).

## 2.3 Operating principles of solar cells

### 2.3.1 Properties of sunlight

The sun has a surface temperature of about 5800 K. Its radiation spectrum can be approximated by a black body radiator at this temperature. There are three mechanisms, which modify the solar spectrum when it travels through the Earth's atmosphere: absorption by gases, Rayleigh scattering by particles that are much smaller than the wavelength, and scattering by aerosols. Thus, the composition and length of the path that light travels in the atmosphere influences the solar flux received on the Earth on a certain location. (Zeghbroeck, 2004) The path length in the atmosphere that the solar radiation passes through in order to reach the Earth's surface is described by air mass (AM). Generally, solar cell performances are compared at AM1.5 (48.2° above the horizon) spectrum normalized to a total power density of 1000 W/m$^2$. The radiation spectra are represented in Figure 2.2.

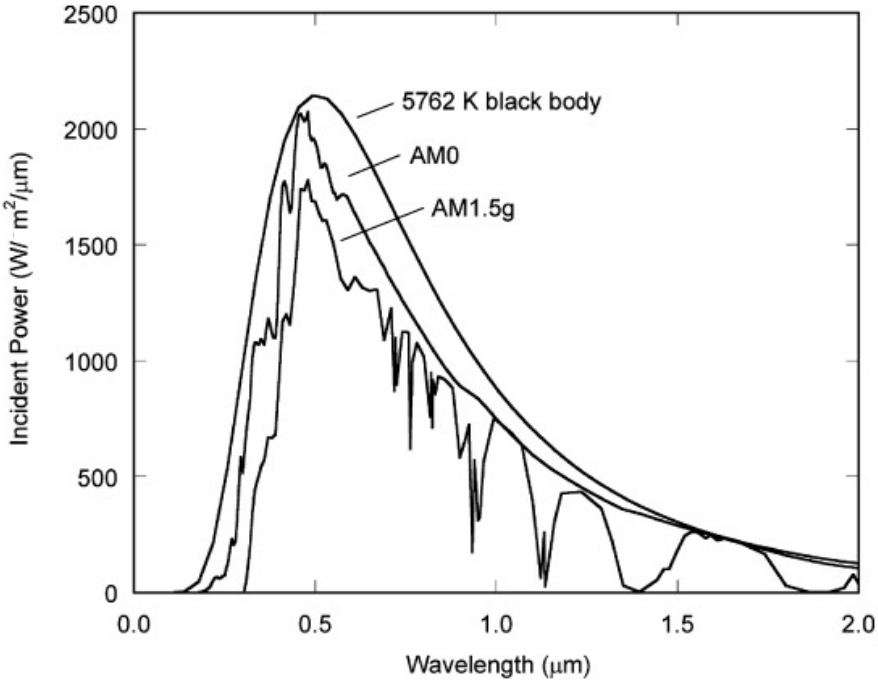


***Figure 2.2.*** *Radiation spectrum for a black body at 5762 K, AM1.5 global spectrum and AM0 spectrum (Luque & Hegedus, 2010).*

AM1.5g refers to AM1.5 global spectrum, indicating that the diffuse component is included in the spectral content of sunlight at Earth's surface. Diffuse component accounts for scattering and reflection in the atmosphere and surrounding landscape. (Luque & Hegedus, 2010)

Sunlight can be considered as consisting of a collection of photons. Photons carry different amounts of energy determined by the spectral properties of their source. Photon energy, defined as $E_{ph} = hf$, where $h$ is Planck's constant and $f$ is the frequency of the wave, corresponds to its wavelength $\lambda$, $E_{ph} = \frac{hc}{\lambda}$, where $c$ is the speed of light in vacuum (Young & Freedman, 2008).

### 2.3.2 Band gap

Crystalline nature of silicon implies that its atoms are aligned in a regular periodic array, known as the diamond lattice. In a single isolated atom, electrons can occupy finite number of energy states. However, in a crystalline structure different energy levels of the individual atoms overlap each other and stretch to form energy bands. The absorption of a photon raises an electron to a higher energy state since a photon is capable of transferring its energy and thus exciting the electron. More specifically, the electron moves from the valence band $E_v$ where it was in a bound state to the conduction band $E_c$ where it is free of bonding and can move around the semiconductor and participate in conduction.

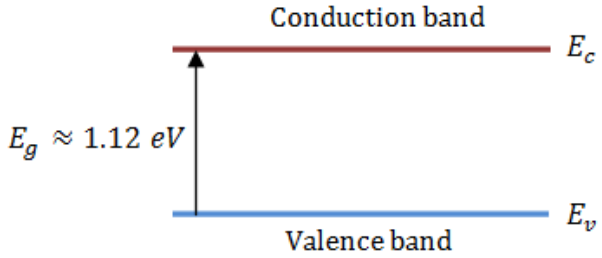


***Figure 2.3.*** *Energy band gap of silicon.*

A photon striking a semiconductor wafer thus generates an electron-hole pair provided that its energy is equal or greater than that of the semiconductor band gap $E_g$ which is a gap in energy between the valence and conducting bands as demonstrated in Figure 2.3. Band gap is the energy range, where no electron state can exist. When an electron is ripped out from the atom through the energy of a photon, it leaves a positive charge behind, called a hole. This process is otherwise known as the electron-hole pair (EHP) generation. Electrons and holes are carriers of electrical current. Holes are also capable of moving through the crystal even though they are not particles. Neighboring electrons are capable of occupying the empty space initially left by an excited electron leaving behind in turn another empty space, which can again be occupied by another neighboring electron causing a so-called ionizing chain reaction. This phenomenon can be viewed as hole movement through the crystal lattice. (Markvart & Castaner, 2004; Luque & Hegedus, 2010)

The photon energy can be insufficient to excite the electron. In such cases the electron will stay in the valence band and the energy is transferred to particles that represent lattice vibrations known as phonons. The insufficient energy is thus converted into heat. On the other hand, photons that have greater energy than the energy bandgap will be absorbed by the semiconductor material, however the difference in energy between the photon energy and the required bandgap energy will be transferred to phonons thus causing thermalization. The energy that can be captured from higher energy photons by a silicon semiconductor device is represented as the gray area in Figure 2.4 under AM1.5 solar spectral conditions (Luque & Hegedus, 2010).

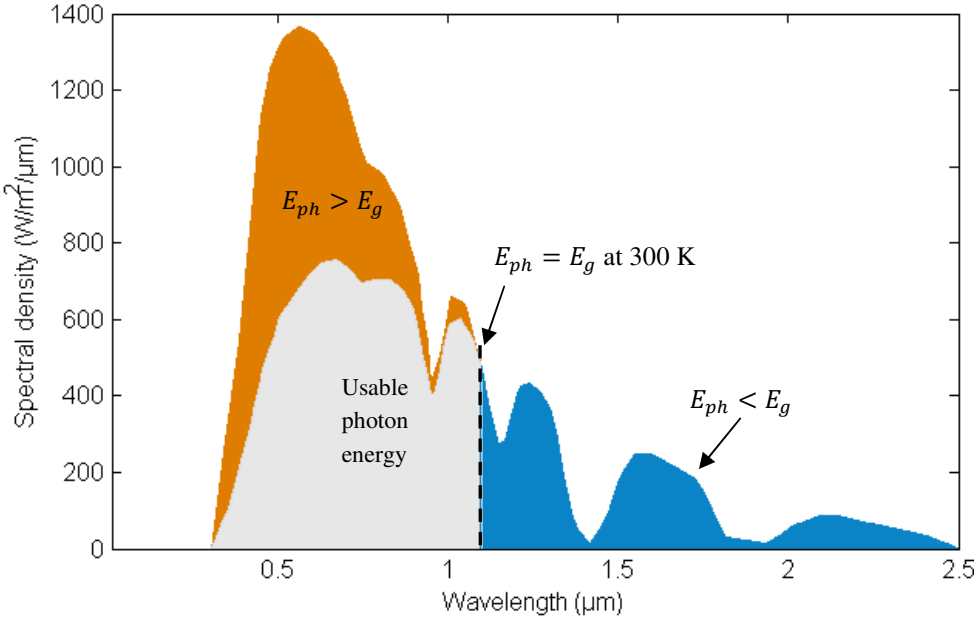


***Figure 2.4.*** *Solar spectrum at AM 1.5. Usable photon energy for a silicon solar cell represented as gray area.*

### 2.3.3 Doping of semiconductors

In the periodic table silicon is in column IV. It thus has four valence electrons, which signifies that four electrons can be shared with the neighboring atoms to form covalent bonds. (Luque & Hegedus, 2010)

In order to vary the number of electrons and holes in semiconductors, specific impurities can be implanted. This technique is otherwise known as doping. The n-type semiconductor materials are produced by implantation of group V dopants, for instance phosphorus, that have one more valence electron than silicon. Hence, the n-type region contains a large number of free electrons. On the other hand, the p-type region contains a large number of free holes due to it being doped with group III elements, most commonly boron, that have one less electron than a silicon atom. Figure 2.5 portrays the negatively and positively doped regions of the cell respectively (Luque & Hegedus, 2010).

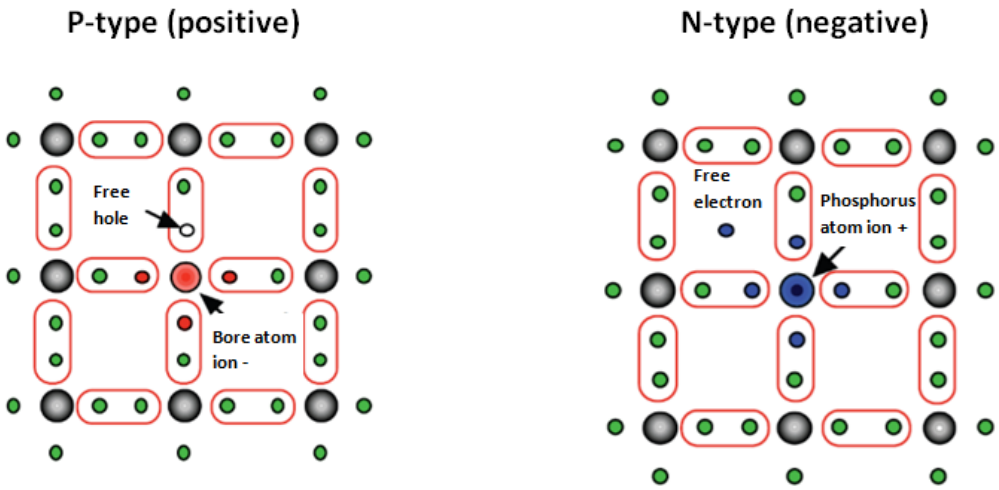


***Figure 2.5.*** *Silicon doping with a bore atom (on the left) and a phosphorus atom (on the right).*

### 2.3.4 p-n junction

In pure semiconductor devices an internal photoelectric effect can generate electron-hole pairs. However, the EHP will directly recombine since there is no force, such as an electric field, to separate the electrons and holes. The p-n junction, formed by joining the n-type and p-type semiconductors, collects photogenerated carriers (created EHP). Therefore, a PV cell is capable of generating power due to a p-n junction that can separate electrons and holes. Free electrons in the n-type semiconductor and free holes in the p-type semiconductor diffuse towards the other side of the junction due to a concentration difference. An electric field is created to prevent the charge carrier diffusion phenomenon and restore equilibrium as shown in Figure 2.6. This region is thus lacking mobile charge carriers (electrons or holes) and is occasionally referred to as the depletion region (Markvart & Castaner, 2004; Luque & Hegedus, 2010; Yagi et al., 2006).

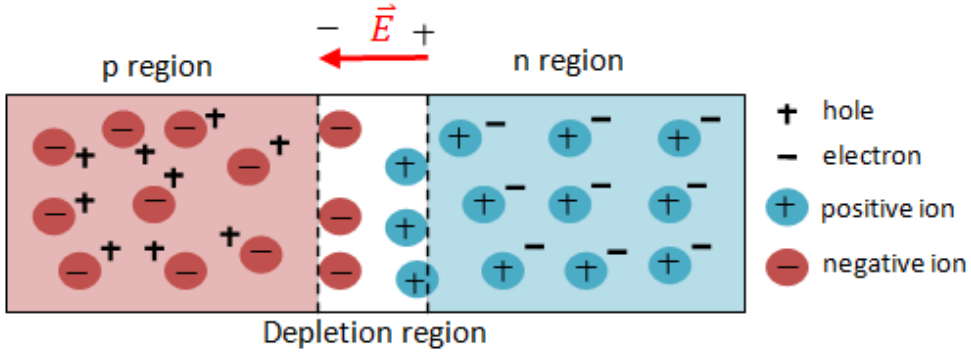


***Figure 2.6.*** *A semiconductor p-n junction.*

### 2.3.5 Photogenerated current

Minority carriers are charge carriers that have lower concentration in a doped material: electrons in the p-type semiconductor material and holes in the n-type semiconductor material. After the incident photon has been absorbed, minority carrier moves by diffusion towards the depletion zone. At the depletion zone they are swept across the junction by a strong electric field and become majority carriers. Naturally, the holes and electrons flow in opposite directions. In other words, the p-n junction prevents recombination by spatially separating the electron and the hole. However, the minority carriers can recombine before reaching the junction (discussed in more detail in Section 2.3.6)

Lastly, if the solar cell is short-circuited, the light generated carriers (higher energy electrons) flow from the solar cell into an external circuit dissipating their energy and finally returning to the cell and recombining with the hole. Metal contacts at the front and back of the cell collect the produced electrical power (Markvart & Castaner, 2004).

The structure of the typical silicon solar cell in use today is demonstrated in Figure 2.7. Most of the incident light is absorbed in the thick base (p-type semiconductor), which forms the bulk of the silicon (Markvart & Castaner, 2004). The base is superposed with the emitter (n-type semiconductor).

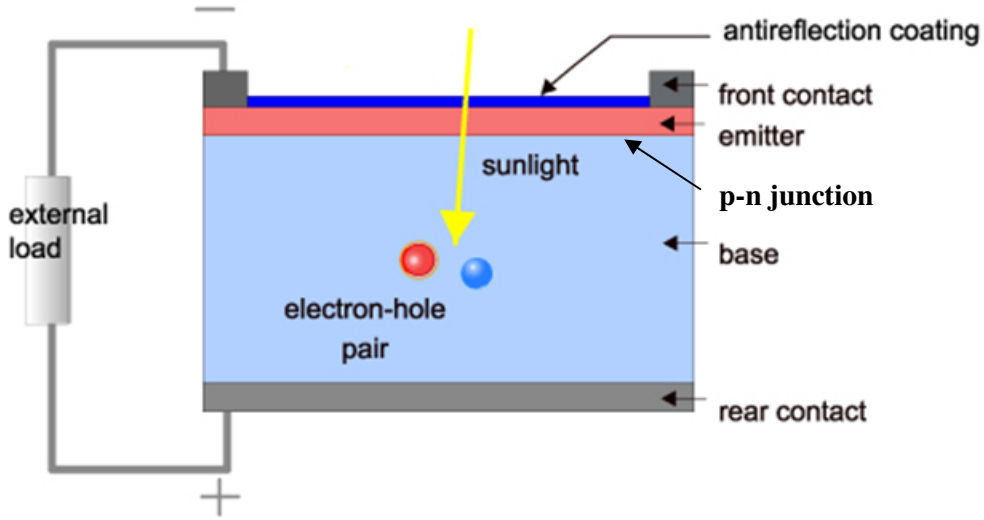


***Figure 2.7.*** *Silicon solar cell structure (Honsberg, 2012).*

### 2.3.6 Recombination

An electron in a conduction band is in a meta-stable state and tends to eventually stabilize to a lower energy position. Recombination is a process when an excited electron returns from the conduction band to the valence lower energy band and thus eliminates the previously created hole (Luque & Hegedus, 2010). Recombination is therefore the opposite process of generation and provokes voltage and current losses. Recombination

of charge carriers can occur in the bulk and on the front and rear surfaces of PV cells. Bulk recombination strongly depends on semiconductor impurities (Fraas & Partain, 2010). There are three recombination mechanisms important from the point of view of solar cell performance that will be discussed next: recombination through traps (defects) in the forbidden gap also known as Shockley-Read-Hall (SRH) recombination, radiative (band-to-band) recombination and, finally, Auger recombination.

### Shockley-Read-Hall recombination

In such trap assisted case of recombination of an EHP, represented as Case 1 in Figure 2.8, the energy of an electron is lost gradually through a two-step relaxation over the energy bandgap. This type of recombination is common in silicon based solar cells, since the distribution of traps in the forbidden energy gaps in the semiconductor material are influenced mainly by impurities and crystallographic defects.

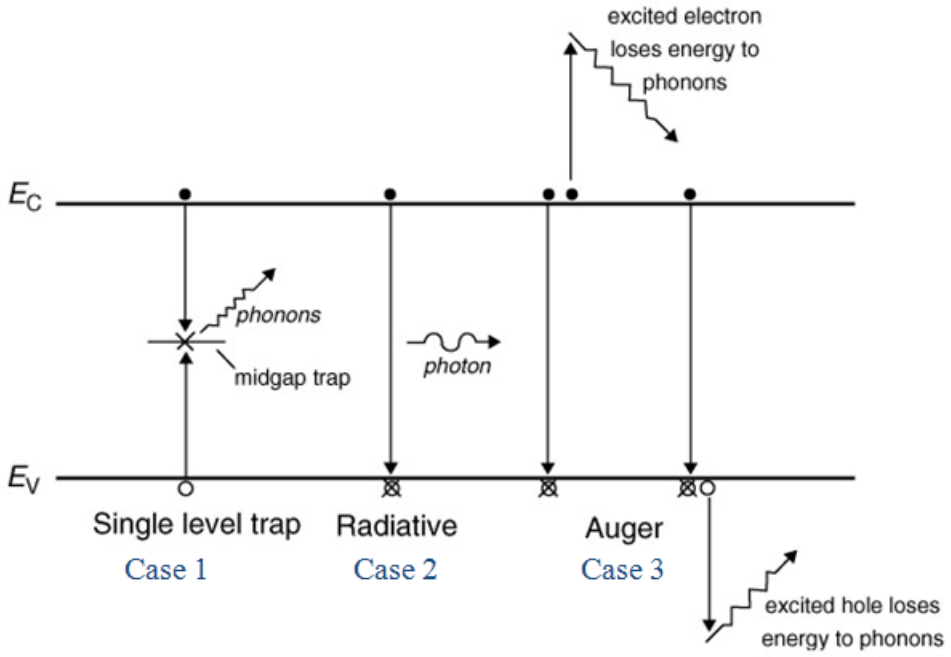


***Figure 2.8.*** *Different recombination mechanisms in semiconductors (Luque & Hegedus, 2010).*

### Radiative recombination

This process, described as Case 2 in Figure 2.8, is exactly the opposite of optical generation process. The energy of an electron descending from the conduction band to a valence band is passed on to an emitted photon. As mentioned previously, most solar cells used in terrestrial applications are made from silicon. However, radiative recombination phenomenon in PV cells made from such semiconductor material is insignificant and is thus usually neglected. Auger and Shockley-Read-Hall recombination, therefore, dominate in silicon-based solar cells. (Luque & Hegedus, 2010)

### Auger recombination

An electron and a hole, and a third carrier, participate in Auger recombination. In such case an electron and a hole recombine and give away the resulting energy to a third carrier (electron or hole) in either the conduction band or the valence band, instead of emitting this energy as heat or photon. If the third carrier receiving the energy is an electron in the conduction band, as illustrated in Figure 2.8 (Case 3), it will experience an increase in kinetic energy, which will later on be lost as the electron relaxes thermally (releases its excess energy and momentum to phonons) descending back to the conduction band edge. Auger recombination plays an important role in highly doped materials, when the carrier densities are high. Increasing the doping level can thus have detrimental effects on the solar cell performance. (Luque & Hegedus, 2010)

### Surface recombination

Despite the fact that recombination is most common at impurities and defects of the crystal structure, it also occurs frequently at the surface of the silicon semiconductor wafer. This is because in general surfaces have a large number of recombination centers due to the interruption of the silicon crystal lattice. Such abrupt termination of the crystal lattice creates dangling bonds (electrically active states) on the silicon semiconductor surface. Furthermore, surfaces have high concentrations of impurities since they are exposed during the fabrication process of the photovoltaic device. (Luque & Hegedus, 2010; Zeghbroeck, 2004)

Due to high recombination rate at the surface, the region is practically depleted of minority carriers, which causes carriers from the surroundings to flow towards this lower concentration region. Surface recombination velocity is a measure used to determine the recombination at the surface, which is dependent on the rate at which the minority carriers flow towards the surface. (Aberle, 2000)

Surface recombination is an important issue specifically in textured silicon solar cells (Aberle, 2000). This is due to the fact that texturing Si solar cells results in an increase in surface area and thus an increase in charge carrier recombination of the semiconductor material (Fraas & Partain, 2010). Nevertheless, several technologies have been developed and introduced into mass production that minimize front surface recombination. Such technologies are referred to as surface passivation. The reader can refer to Aberle (2000) for more information on surface passivation.

### Diffusion length

Diffusion length is determined as the average distance that light-generated minority carriers can travel from the point of generation to the point of collection (p-n junction) (Fraas & Partain, 2010). In the doped semiconductor material, minority charge carrier transport is dominated by diffusion. The diffusion length, $L_{abs}$, of minority carriers in the absorber is, therefore, an important factor when determining the efficiency of a Si

solar cell (Luque & Hegedus, 2010). If the diffusion length is much smaller than the base thickness, the overall efficiency of the PV cell decreases. This is because the light-generated carriers, created too far away from the collection region, have a smaller chance to be collected. High doping level causes diffusion length to become shorter since Auger and Shockley-Read-Hall (SRH) recombinations increase. As mentioned earlier, these types of recombination are dependent, among other things, on the concentration of dopant atoms (Luque & Hegedus, 2010).

Modern high-efficiency solar cells usually have diffusion length that is greater than the base thickness, which increases the ability of the cell to collect near-bandgap photons (Basore, 1990) and thus has a beneficial effect on the cell's QE (see Section 2.5). For monocrystalline silicon solar cells the diffusion length is usually 100-300 μm, while the base thickness is typically 100-500 μm.

## 2.4 Optical losses

Optical losses provoke low incident photon absorption and thus play an important role in limiting the conversion efficiency of solar cells. Large refractive index of silicon is partly responsible for its poor optical properties as a semiconductor material. In fact, about 36 % of incident light in the wavelength range of 0.4-1.2 μm is reflected from the front-face of bare Si (Yagi et al., 2006). Such high front-face reflectance implies that this amount of light is not able to penetrate the solar cell, as illustrated in Figure 2.9.

Another contribution to optical losses of PV cells happens when a fraction of light, especially with long absorption lengths, is lost due to so-called parasitic absorption in non-photo active material, such as the rear reflector. Furthermore, the amount of incident flux that can potentially enter the silicon is diminished due to the shading effects of the front electrodes.

Nevertheless, silicon solar cells of conventional design are sufficiently thick to absorb most of the light before it reaches the back surface. The top contact coverage of the cell surface can also be minimized. As a result, the focus has traditionally been on decreasing front-face reflectance. (Honsberg, 2012; Yagi et al., 2006)

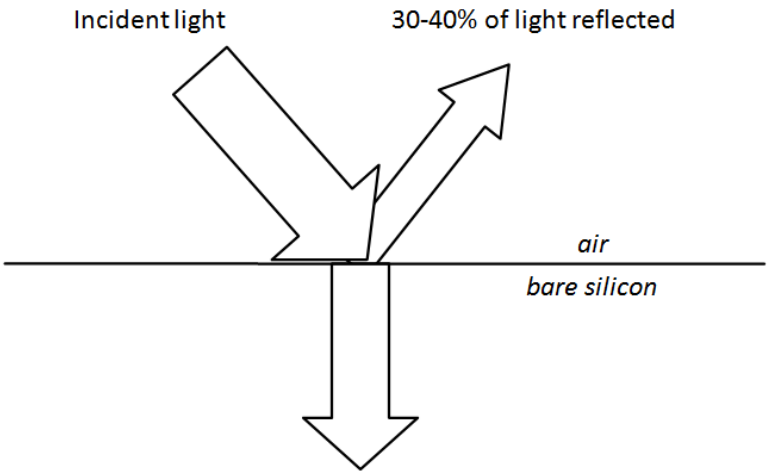


***Figure 2.9.*** *Light reflected from bare silicon substrate.*

In order to understand how light behaves between two media with different optical properties and why such a large fraction of light is reflected from the front-face of bare silicon, some optical basis described in Sections 2.4.1 and 2.4.2 is required.

### 2.4.1 Principles of geometrical optics

Light exhibits a paradox behavior known as the wave-particle duality implying that it has both particle (photons) and wave properties. Due to this reason there are two analytical approaches when studying reflection and transmission of electromagnetic waves on a surface: wave-optics approach and geometrical approach. Geometrical optics regime considers light as rays, whereas physical optics is based on wave-theory (Young & Freedman, 2008; Torrance & Sparrow, 1967). Physical optics can thus account for interference and diffraction effects. Since the model chosen to simulate the reflection of a textured Si solar cell (described in more detail in Section 4.3) is based on geometrical optics, a theoretical basis for such optics regime will be covered in this section.

#### Refractive Index

The refractive index, denoted as $n$, describes how light propagates through a medium and it represents the ratio of the speed of light $c$ in a vacuum to the speed $v$ in the material.

$$n = \frac{c}{v} \tag{2.1}$$

Wave speed is inversely proportional to the index of refraction. Hence, the greater the refractive index, the slower the wave speed in the medium (Young & Freedman, 2008). Ray propagation velocity can be expressed as a function of electrical and magnetic properties of the medium

$$v = \frac{1}{\sqrt{\varepsilon\mu}} \tag{2.2}$$

where $\varepsilon$ is electrical permittivity and $\mu$ is magnetic permeability.

Electromagnetic waves do not attenuate in a perfect non-absorbing dielectric medium. Such materials are referred to as nonconductors. Attenuation indicates that there is energy absorption from the waves as they travel through the medium. Naturally, crystalline silicone medium is an attenuating medium, since it is classified as a semiconductor. The refractive index of silicon has to be substituted by a complex refractive index, $\bar{n}$, which has a real component and a complex component, as seen in the following equation

$$\bar{n} = n - ik \tag{2.3}$$

where $k$ is the extinction index of wave in a medium. However, in this thesis it is assumed that the complex part of the refractive index plays an insignificant role in determining the Fresnel's coefficients that are required in order to obtain the reflectance and transmittance of an air/silicon interface, later described in Section 2.4.2 (Siegel & Howell, 2002). Hence, only the real part of the refractive index of silicon is considered.

Figure 2.10 represents the distribution of refractive index values of silicon in terms of wavelength (Polyanskiy, 2013): the top figure represents the refractive index of silicon on a wider wavelength range and the bottom figure represents the refractive index distribution on a wavelength range that is more significant to a silicon solar cell (corresponds to the near bandgap region).

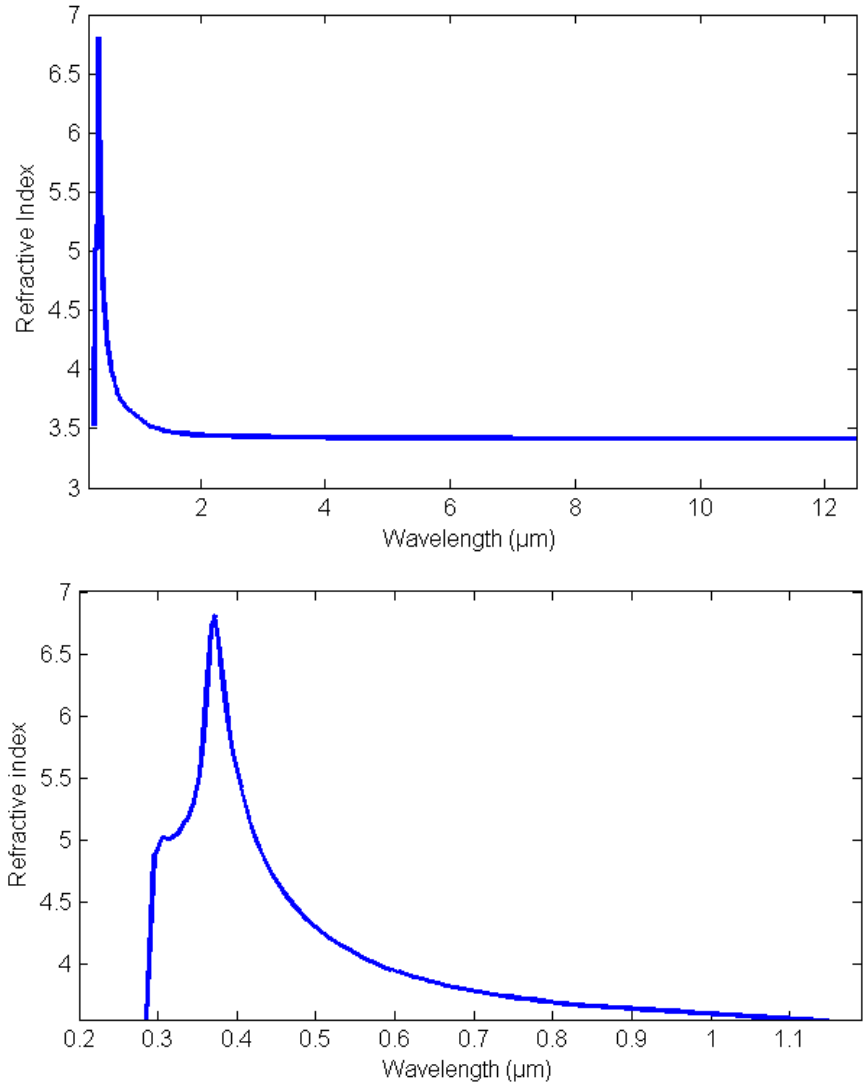


***Figure 2.10.*** *Refractive index of silicon as a function of wavelength.*

From the graphs it can be seen that at the wavelength value of approximately 0.37 µm the refractive index reaches a peak value of 6.8 after which is reaches a nearly constant value of approximately 3.5.

In the upcoming sections the importance of refractive index will be highlighted when determining the reflectance and transmittance of textured and smooth surfaces.

### Snell's Law

When an incident light encounters an interface between two media, it can undergo absorption, reflection, interference, and scattering before it is transmitted into the bulk of the second medium (Young & Freedman, 2008). From the point of view of solar cell performance analysis it is particularly interesting how much light is reflected from the silicon surface.

Light is considered to be reflected specularly if it is reflected from a smooth surface at a definite angle. The angle of reflection is equal to the angle of incidence for all

wavelengths and for any pair of materials. Rough surfaces, such as textured surfaces, can cause diffuse reflection to occur signifying that light will be reflected in a scattered manner. However, reflection from a rough or textured surface can still be approximated as distinct specular reflections, when investigating the reflection on a microscopic scale and referring to a ray tracing approach (Baker-Finch & McIntosh, 2010; Torrance & Sparrow, 1967; Smith & Rohatgi, 1993). This approach is described in more detail in Section 4.3.

Snell's law establishes a relation between the angle of refraction (transmission), $\theta_{tj}(°)$, and the angle of incidence, $\theta_j$, through the ratio of refractive indices (Siegel & Howell, 2002) demonstrated in the following equation

$$n_1 sin\theta_j = n_2 sin\theta_{tj} \tag{2.4}$$

where $n_1$ is the refractive index of one medium and $n_2$ is the refractive index of another medium. The equation also portrays that when a ray passes through medium 1 to another medium 2, that has a greater index of refraction ($n_2 > n_1$), i.e. where the propagation of light is slower, as in the case of light propagating from air to silicon, the angle $\theta_{tj}$ is smaller in the second medium than the incident angle in the first medium $\theta_j$. On the other hand, if the medium 2 has a smaller index of refraction than the first medium, ($n_1 > n_2$), the refracted ray bents away from the normal. Furthermore, in such cases when $n_1 > n_2$ total internal reflection can occur, assuming that the angle of incidence exceeds a critical angle, $\theta_{crit}$, determined by

$$sin\theta_{crit} = \frac{n_2}{n_1} \tag{2.5}$$

Total internal reflection signifies that all light is reflected. (Young & Freedman, 2008)

In this study we consider that light propagates from air directly towards the crystalline silicon surface, which has a larger refractive index at any wavelength than the refractive index of the first medium, air. Therefore, in such configurations the occurrence of total external reflection is not possible. However, it should be noted that at relatively large incident angles, the reflected fraction of incident light is very large and in some cases can be approximated as all light being reflected (Siegel & Howell, 2002).

### 2.4.2 Reflection

#### Polarization

According to the wave theory light is a transverse electromagnetic wave, which is combined of oscillating electric and magnetic fields. When light waves oscillate in a single plane, light is considered to be polarized. The polarization angle $\varphi$ is defined as the angle between the positive horizontal axis and a vector parallel to the incident electric field, $E_i$, and it represents the perpendicular or $\hat{s}$ -polarization state. The angle $\varphi + \frac{\pi}{2}$ represents the parallel polarization or $\hat{p}$ -polarization state. Any state of polarization can

be defined as a function of the $\hat{s}$- and $\hat{p}$ -polarizations (Siegel & Howell, 2002) and McIntosh) represented in Figure 2.11.

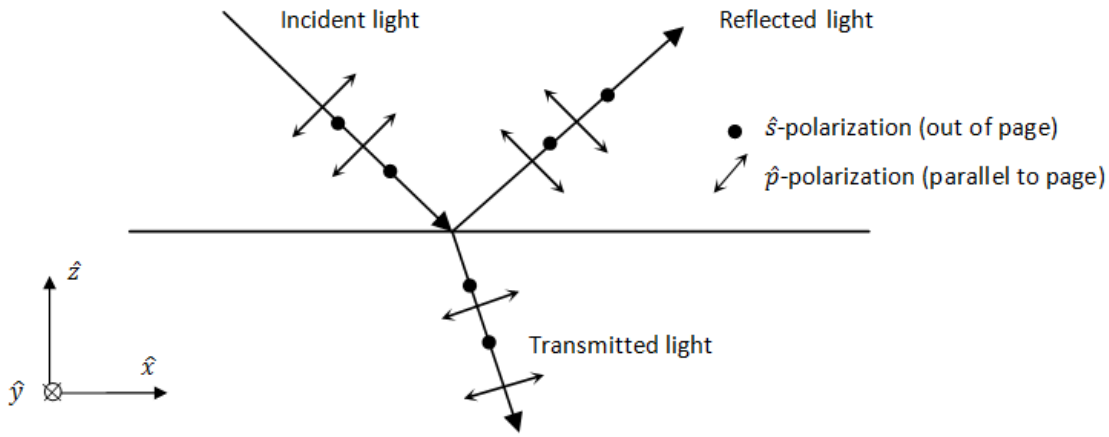


***Figure 2.11.*** *Parallel and perpendicular polarization states of incident, reflected and transmitted light.*

The plane of incidence is in the $\hat{x}\hat{z}$ -plane of a Cartesian coordinate system $(\hat{x}, \hat{y}, \hat{z})$.

The following equation represents the light flux that is reflected from an interface

$$I_r = \frac{1}{2\pi}\int_0^{2\pi} \|E_r(\varphi)\|^2 d\varphi \tag{2.6}$$

where

$$E_r(\varphi) = rE_i(\varphi) \tag{2.7}$$

and $r$ is the reflection coefficient described in more detail later in this section. Finally, the incident electric field, $E_i(\varphi)$, is represented with the following equation

$$E_i(\varphi) = (\cos\varphi)\hat{x} + (\sin\varphi)\hat{y} \tag{2.8}$$

The integral over the polarization angle $\varphi$ in Equation 2.6 represents the uniform distribution of unpolarized light (Baker-Finch & McIntosh, 2010). When light wave is vibrating in more than one plane it is considered to be unpolarized. Unless sunlight is filtered, it is generally considered to be unpolarized.

In order to obtain the reflected flux for the unpolarized light Equation 2.6 can be simplified as follows

$$I_r = \frac{1}{2}\left(\|E_r(\varphi)\|^2 + \left\|E_r(\varphi + \frac{\pi}{2})\right\|^2\right) \tag{2.9}$$

or

$$I_r = \frac{1}{2}\left(\|E_r|_{\hat{s}}\|^2 + \left\|E_r|_{\hat{p}}\right\|^2\right) \tag{2.10}$$

representing the average of two perpendicular polarizations. (Siegel & Howell, 2002; Young & Freedman, 2008)

### Fresnel's Law

Fresnel's equations give the ratio of the amplitude of reflected/transmitted electric field to initial electric field for electromagnetic radiation that is incident on a dielectric non-absorbing medium. Essentially, Fresnel's equations give reflection and transmission coefficients for waves that are parallel and perpendicular to the incidence plane at the interface of two media with different refractive indices. The reflection coefficient for perpendicularly polarized light is

$$r_{\hat{s}} = \frac{E_{\hat{s},r}}{E_{\hat{s},i}} = -\frac{n_2 cos\theta_{tj} - n_1 cos\theta_j}{n_2 cos\theta_{tj} + n_1 cos\theta_j} \tag{2.11}$$

and the reflection coefficient for parallel polarized light is

$$r_{\hat{p}} = \frac{E_{\hat{p},r}}{E_{\hat{p},i}} = \frac{n_2 cos\theta_j - n_1 cos\theta_{tj}}{n_2 cos\theta_j + n_1 cos\theta_{tj}} \tag{2.12}$$

The fraction of incident power reflected, otherwise known as reflectance $\rho$ can be derived from the reflection coefficient and is thus equal to $r^2$. It is represented in the following equations for perpendicularly and parallel polarized light respectively

$$\rho_{\hat{s}} = r_{\hat{s}}^2 = \frac{sin^2(\theta_j - \theta_{tj})}{sin^2(\theta_j + \theta_{tj})} \tag{2.13}$$

$$\rho_{\hat{p}} = r_{\hat{p}}^2 = \frac{tan^2(\theta_j - \theta_{tj})}{tan^2(\theta_j + \theta_{tj})} \tag{2.14}$$

and for non-polarized waves from equation 2.10

$$\rho = \frac{\rho_{\hat{s}} + \rho_{\hat{p}}}{2} \tag{2.15}$$

### Energy conservation law

The sum of energy of the wave that is transmitted and energy of the wave that is reflected is equal to the energy of the original wave. The balance of energy flux on an interface can be represented by the following equation

$$\rho + t = 1 \tag{2.16}$$

where $t$ is transmittance. Figure 2.12 is a graphical illustration of light incident on an interface, where $I_0$ represents the intensity of the incident light, $I_r$ reflected light, $I_t$ transmitted light and $n$ is the normal of the interface. (Siegel & Howell, 2002)

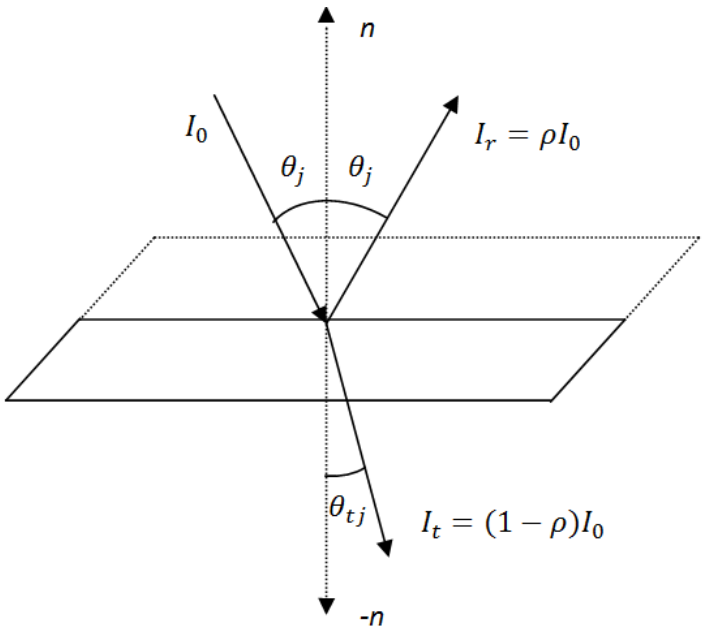


***Figure 2.12.*** *Incident, reflected and transmitted electromagnetic waves at the interface of two media with different optical properties.*

The fact that the value of the refractive index does not vary significantly when the wavelength is greater than 1.2 µm, as seen in Figure 2.10, indicates that the reflectance and transmittance obtained from Equations 2.4 and 2.13-2.16 do not change significantly either at the same wavelengths.

## 2.4.3 Absorption coefficient of silicon

The wavelength-dependent absorption coefficient of silicon determines its absorbing properties. Light that is not reflected from the front-surface of the silicon is thus transmitted into the semiconductor, attenuates inside the material, according to the equation

$$I(\hat{z}) = I_0 e^{-\alpha z} \tag{2.17}$$

where $I(\hat{z})$ is the intensity of the light after attenuation due to its passage over a distance $z$ in the silicon, and $\alpha = \frac{4\pi f k}{c}$ is the absorption coefficient. (Siegel & Howell, 2002)

The wavelength dependence of the absorption coefficient of silicon is shown in Figure 2.13 (Green, 2008). It can be seen that at small wavelength the coefficient is extremely high. This signifies that light is absorbed within the first 0.010 µm of its passage through the silicon. As mentioned before, the energy of photons at such wavelength is much higher than the energy bandgap of silicon. (Hylton, 2006)

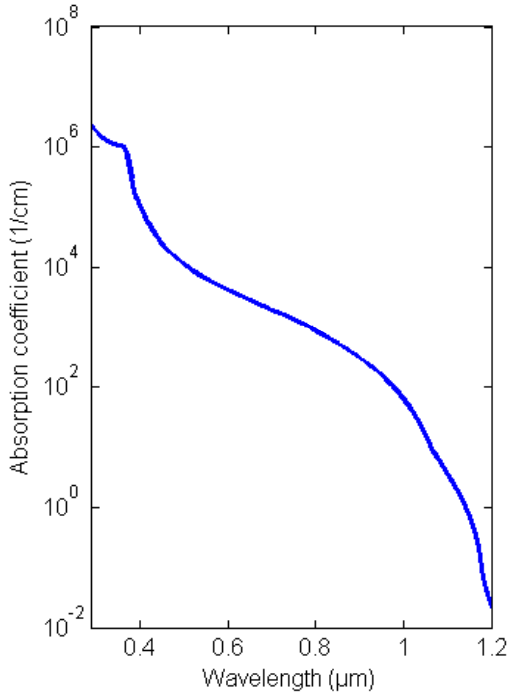


***Figure 2.13.*** *Absorption coefficient of pure silicon (300 K).*

The photon energy becomes too small at longer wavelengths to provide a direct excitation (without the assistance of phonons) of an electron. For wavelengths above 1.1 µm the absorption coefficient decreases to zero and electron-hole pairs are no longer generated. Silicon material becomes in this case transparent for long wavelength photons.

## 2.5 Quantum efficiency

Quantum efficiency represents the probability of an electron generated and collected under the short-circuit conditions from an incident photon on a semiconductor material. It thus describes the electrical sensitivity of a photovoltaic device to incident light. QE measurements provide researchers with such data as overall device performance and material purity. The same mechanisms that affect the minority carrier collection probability also affect the QE. Naturally, in order to improve the conversion efficiency of a solar cell QE has to be raised. (Basore, 1990; Yang et al., 2008)

QE considers external quantum efficiency (EQE) and internal quantum efficiency (IQE). The main difference between internal quantum efficiency and external quantum efficiency is that IQE takes into account only the portion of light that actually enters the solar cell and is not lost by front surface reflection. Since EQE includes the effects of optical losses due to reflection, it is lower in value than IQE. The values of EQE and IQE are routinely measured using interference filters or monochromators in order to assess the performance of a solar cell. (Markvart & Castaner, 2004)

Quantum efficiency is often expressed as a function of wavelength, since the energy of a photon is inversely proportional to its wavelength. If the energy of a photon is below band gap energy of silicon ($E_g \approx 1.12\ eV$ at 300 K), QE is zero, since such photons are unable to create an electron-hole pair. This can be seen from Figure 2.14, where at longer wavelengths ($\lambda > 1.1\ \mu m$) photons are not absorbed and thus all solar energy is lost. (Fraas & Partain, 2010; Luque & Hegedus, 2010) At shorter wavelength, photons transport more energy than needed. However, they still produce only one electron that will move, if not recombined, through a voltage of no more energy than the bandgap energy (Fraas & Partain, 2010). QE at these wavelengths will ideally be equal to one. Since QE is the ratio of the number of collected charge carriers and the number of incident photons, it thus does not account, for instance, for the effect of thermalization in solar cells produced from photon's excess energy.

In an ideal case, QE of a solar cell device has a square shape, as shown in Figure 2.14. Nevertheless, due to recombination effects and reflection losses, the QE for most solar cells is reduced. Since shorter wavelengths (high energy light) are absorbed closer to the surface they are subjected to surface recombination which decreases the QE. Longer wavelengths, such as green light, on the other hand are absorbed deeper in the bulk. Minority carriers will be forced to travel longer paths before they are collected and therefore low diffusion lengths will reduce the QE at these wavelengths (Zeghbroeck, 2004; Tiedje et al., 1984).

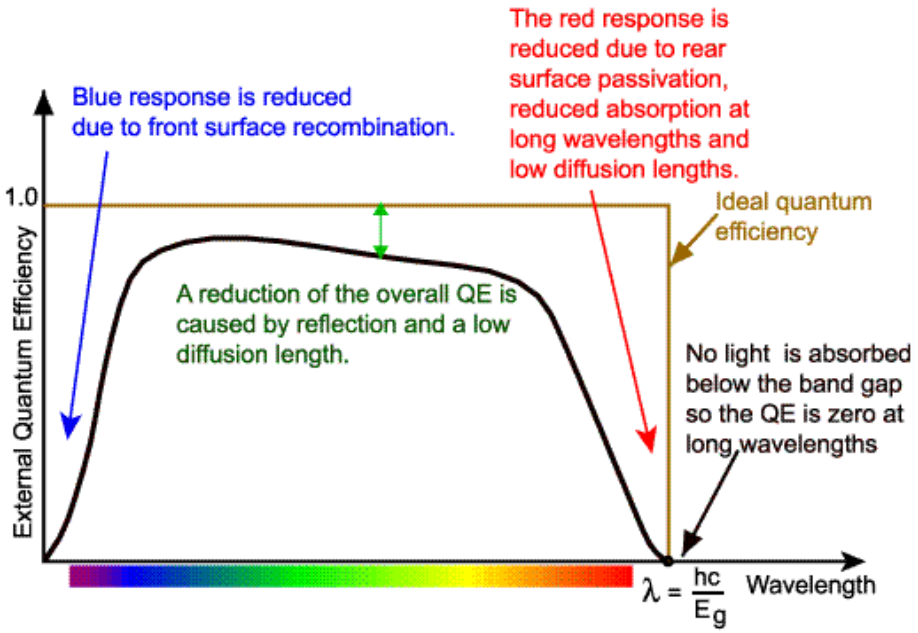


***Figure 2.14.*** *Ideal and measured external quantum efficiency of a silicon solar cell (Honsberg, 2012).*

Studies have shown that quantum efficiency is higher in monocrystalline silicon solar cells than in multicrystalline silicon (mc-Si) solar cells. This highlights the importance of using monocrystalline silicon material for high efficiency solar cells (Fraas & Partain, 2010). The reason why c-Si cells tend to have higher QE values is because in mc-Si carrier recombination is greater than in monocrystalline due to recombination at the grain boundaries. (DiStefano, 2009) As mentioned earlier in Section 2.3.6 grain boundaries that favor imperfections, such as impurities and crystallographic defects, increase Shockley-Read-Hall and Auger recombinations. (DiStefano, 2009) Recombination is also increased in mc-Si due to the defects related to the manufacturing process of such silicon semiconductors.

### 2.5.1 Internal quantum efficiency

Internal quantum efficiency provides a superior analysis when studying solar cell performance, since only the photons that are absorbed and not reflected from the front surface potentially contribute to the light generated current $J_L$ (Basore, 1990). In most solar cells light generated current is equal to the short-circuit current $J_{sc}$ and is the largest current that can be drawn from a cell. Readers can refer to Zeghbroeck, (2004) and Yagi et al., (2006) for further information about electrical properties of silicon solar cells.

Internal quantum efficiency analysis increases the understanding not only of recombination parameters that govern the solar cell performance, such as diffusion length and recombination velocity, but also the performance limitations imposed by other optical losses than front surface reflection. (Basore, 1990; Brendel et al., 1996)

Spectrally resolved internal quantum efficiency can be obtained from the following equation (Basore, 1990)

$$IQE = SR \cdot \frac{hc}{\lambda} \cdot \frac{1}{q(1-\rho)} \tag{2.18}$$

where $h \approx 6.63 \cdot 10^{-34} m^2 kg/s$ is the Planck's constant, $\lambda$ is the free-space wavelength, $q$ is the elementary unit charge and SR represents the spectral responsivity in a solar cell. Determining the internal quantum efficiency with the help of Equation 2.18 involves measuring/calculating the cell's spectral response and front surface reflectance $\rho$ at different wavelengths. The term $(1-\rho)$ normalizes the IQE to the fraction of photons that are not reflected by the cell. When attempting to improve the IQE, reflection losses of a cell at the front-surface must be minimized. Combining an antireflection coating (ARC) and some type of texturing technique (discussed in more detail in Chapter 3) can potentially decrease the front-face reflectance close to zero. However, as mentioned earlier the IQE and thus the overall performance of the solar cell can also be affected by the non-unity back surface reflectance $\rho_{bs}$ (parasitic absorption in non photoactive material) and non-unity internal surface reflectance $\rho_{in}$ (see Section 3.2), since they decrease the light intensity without EHP generation. (Basore, 1990; Bücher et al., 1994)

It was pointed out by Brendel et al. (1996) that when calculating internal quantum efficiency using a theoretical model one has to consider contributions from all important current generation regions

$$IQE = \sum_{i=e,scr,b} IQE_i \tag{2.19}$$

where $e$ is the emitter region, $scr$ is the space charge region or otherwise known as depletion region and $b$ is the base region (Brendel et al., 1996). Considering current generation not only in the base region is especially crucial for very thin cells, since the wavelength region of light that is mainly absorbed in the base of the cell becomes very small. Therefore, an approximation made in many studies where the IQE of a solar cell is analyzed considering current generation only in the base of the cell is more applicable to conventional thick Si solar cells represented in Figure 2.7 (discussed in more detail in Section 4.4).

### 2.5.2 Spectral response

The ratio of the short-circuit current generated by a solar cell under monochromatic illumination of a given wavelength and the spectral irradiance at the same wavelength is represented by spectral response $SR$ in Equation 2.20.

$$SR = \frac{J_{sc}}{I_{light}} \tag{2.20}$$

where $I_{light}$ is the power incident on the solar cell as a function of wavelength. Spectral response thus represents how efficiently the solar cell converts light into short-circuit current at various wavelengths. Reliable spectral response data on p-n junction of silicon solar cells can indicate the absorption behavior of the cell (Luque & Hegedus, 2010; Terman, 1961). SR is expressed in amps per watts; A/W. Depending on the value used for the quantum efficiency, spectral response can also be either internal or external. Furthermore, spectral response is conceptually somewhat similar to quantum efficiency. (Markvart & Castaner, 2004; Yang et al., 2008) Just as QE, the ideal SR is limited at long wavelengths due to a silicon semiconductor device being unable to absorb such low energy photons. However, the difference between spectral response and quantum efficiency is that SR does not have a square shape in an ideal case. Instead, the SR first linearly increases as the wavelength increases reaching a maximum, where spectral responsivity is at its highest corresponding to wavelengths where $E_{ph} \approx E_g$. The SR at short wavelengths is low since only one EHP can be generated and collected at short wavelengths, where $E_{ph} > E_g$, and the excess energy is released as heat. After reaching a peak, the SR of cell rapidly decreases, due to the fact that in silicon solar cells no EHP can be generated when $E_{ph} < E_g$. (Sinton & Cuevas, 1996; Luque & Hegedus, 2010)

To conclude both spectral responsivity and quantum efficiency are essential in understanding current generation, recombination and collection mechanisms in PV cells (Luque & Hegedus, 2010).

# 3 SURFACE TEXTURES

## 3.1 Introduction

As mentioned in Chapter 2, due to poor optical properties of silicon, reflection losses deteriorate the conversion efficiency of solar cells (Chen & Wang, 2011). This chapter will introduce surface textures as means of decreasing front-face reflection. Section 3.2 will explain how surface textures decrease the reflection from the front surface and increase light absorption. Different structure types created by texturing silicon PV cells and their dimensions will also be mentioned. In Section 3.3 various texturing techniques dependent on the structure of the silicon material are presented. The disadvantages of surface textures are briefly discussed in Section 3.4. Finally, the impacts of textures on the QE of a cell are explored in Section 3.5.

## 3.2 Light trapping

Texturing the surface of wafer-based Si solar cell is one of the techniques used to decrease the front-face reflectance and thus enhance the level of absorption of incident light. Texturing can also improve light absorption within the bulk of the cell by absorbing photons closer to the collection junction and by making use of weakly absorbed near-bandgap light. (Gjessing, 2012; Basore, 1990) Depending on the texturing technique and the crystallographic orientation of silicon surface planes there is a number of different types of texture morphologies produced on silicon surfaces (Gjessing, 2012; Honsberg, 2012). The most commonly created structures are regular upright or inverted pyramids, random upright pyramids and grooves. Figure 3.1 and Figure 3.2 demonstrate regular upright pyramids and periodic grooves or otherwise known as V-shaped trenches.

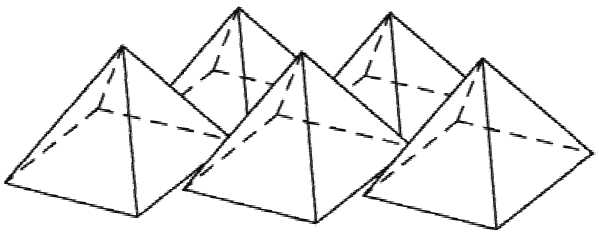

***Figure 3.1.*** *Regular upright pyramids as surface textures (Honsberg, 2012).*

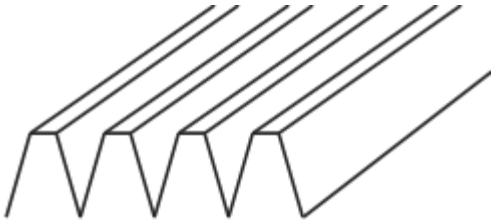

***Figure 3.2.*** *Periodic grooves with flat tops as surface textures.*

Created textures decrease the overall reflectance due to three distinct mechanisms. First, a portion of light that is incident on the Si wafer is reflected from the angled surface, striking another angled surface. This phenomenon illustrated in Figure 3.3 as case 1 is referred to as multiple reflections or multiple light bounces. It increases the amount of transmitted solar flux and thus the probability of photon absorption, since initially reflected photons will have at least one other chance to enter the solar cell (Gjessing, 2012; Smith & Rohatgi, 1993; Jha, 2010).

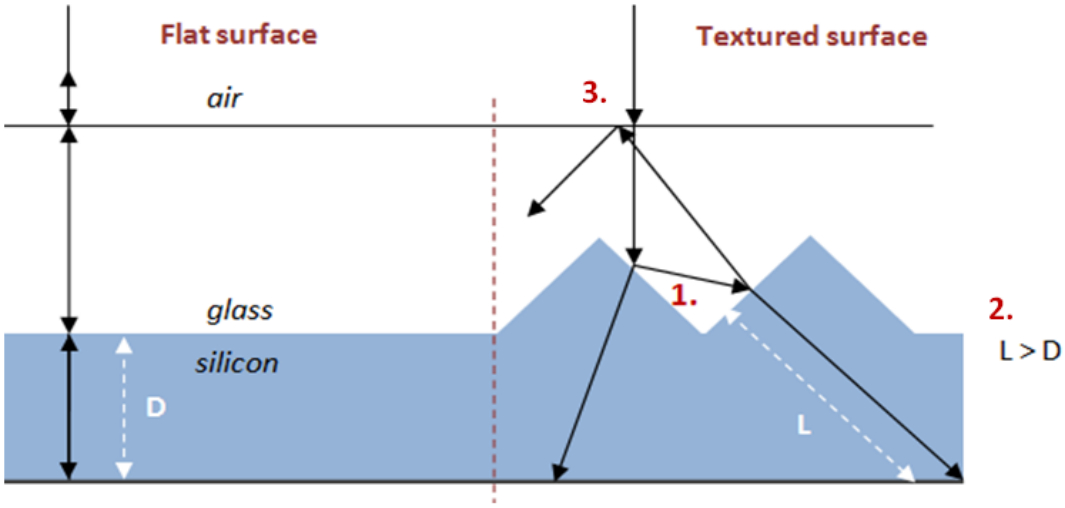


***Figure 3.3.*** *Normally incident light behavior on a textured surface (on the right) in comparison with a flat surface (on the left).*

Longer path length of the refracted light carrying photons is the second reason for increased photon absorption and absorption closer to the collection junction. Normally incident light propagates within the bulk of the silicon at an angle in textured solar cells. This results in longer path lengths that light will travel before reaching the rear surface, as opposed to the path length of normally incident light refracted from a flat surface (see Figure 3.3, case 2). (Basore, 1990) This is especially important if the diffusion lengths are comparable to or less than the cell thickness (Macdonald, et al., 2004).

Finally, increased total internal reflection probability also increases the overall transmitted flux since it does not permit the light from escaping from the silicon material (Figure 3.3, case 3). This phenomenon is also known as light-trapping. Long-wavelength photons that the semiconductor material was unable to absorb are reflected

from the back surface to the front. There they encounter once again an angled surface and with an appropriate incident angle, they undergo total internal reflection, described in Section 2.4.1, either at the silicon interface or at the glass surface. (Gjessing, 2012; Macdonald, et al., 2004)

Because of poor optical properties of silicon material, the thickness of solar cells has to be relatively large in order to absorb 99 % of the solar spectrum, which leads to an increase in weight, production cost and recombination probability in the bulk. However, since light absorption is enhanced in textured cells, the thickness of such cells can remain relatively small. (Chen & Wang, 2011)

Some other techniques, such as antireflection coatings can be used to reduce front-face reflection. ARC is a thin layer of an optimal thickness of dielectric material. This layer cancels the reflected beams by interference. In fact, texturing can be in combination with an ARC. Such configuration can produce even lower solar cell reflectance than each of these methods separately.

## 3.3 Texturing techniques

There are three types of texture configurations on Si solar cells: both faces textured (BOFT), front face textured (FFT) and back face polished, and finally back face textured (BAFT) with front face polished (Verlinde et al., 1992; Rodriguez et al., 1997).

Roughening of the silicon surface can produce different types of textures. Regardless of the crystallographic orientation of silicon wafer planes, different types of etching techniques are used to create these surface textures. Such techniques are wet etching with alkaline or acidic solutions, reactive-ion etching (RIE) and mechanical etching. The choice of the etching technique depends on whether the silicon material used is monocrystalline or multicrystalline (Yagi et al., 2006; Gjessing, 2012; Honsberg, 2012). Sections 3.3.1 and 3.3.2 describe the texturing techniques for monocrystalline and multicrystalline silicon solar cells and structures produced when employing such techniques. Readers can refer to Xi et al., (2004), Panek et al., (2005) and Fukui et al., (1997) for more detailed information.

### 3.3.1 Texturing monocrystalline silicon solar cells

Monocrystalline silicon can be textured by employing wet etching techniques along the faces of the crystal planes. There is a chemical reaction between various inorganic alkaline solutions and silicon, provided that the solution temperature is high enough. (Chen & Wang, 2011) Alkaline solutions used are typically low concentration sodium hydroxide (NaOH) or potassium hydroxide (KOH) solutions. These etching solutions have an anisotropic nature and require a specific crystal plane orientation of (100) at the surface. The anisotropic nature of these solutions implies that the corrosion rate is dependent on the crystallographic orientations of surface planes. Silicon surface planes with a (100) are the easiest to break and thus etch much faster. On the other hand, surface planes with a (111) orientation etch much slower than the rest of the planes. Hence, when etch-

ing a crystalline silicon surface with an anisotropic solution, the result is a random pattern of pyramids where the (111) surface planes form the pyramid walls. (Gjessing, 2012) Figure 3.4 is a graphical representation of such textures.

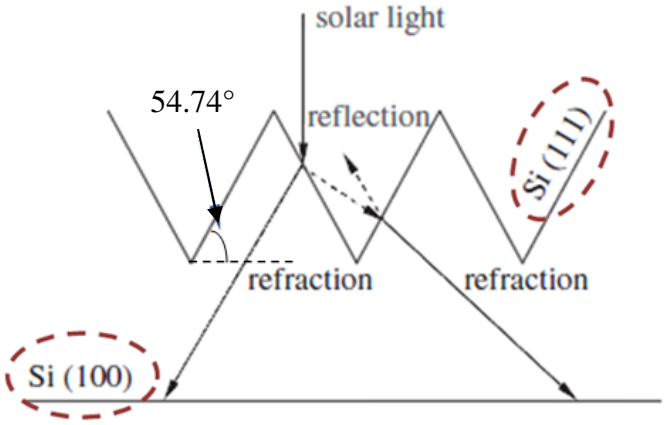


***Figure 3.4.*** *Anisotropic etching revealing (111) wafers on crystalline silicon surface (Yang et al., 2006).*

Created pyramid structures with a (111) orientated facets have a 54.74° facet tilt angles. The facet tilt angle is the angle formed by the base of the pyramid and the lateral edge, as shown in Figure 3.4. The facet tilt angle of 54.74° is determined by the crystal structure of the silicon. (Gjessing, 2012; Bressers et al., 1996) If the incident light is reflected at the first bounce from a pyramid with such facet tilt angle, it will always receive a second chance to enter the silicon substrate as it hits another pyramid wall. Therefore, such pyramids are capable of efficiently reducing front-side reflectance. (Singh et al., 2001; Bean, 1978)

Texturing monocrystalline cells is thus a relatively simple process, and is easier than texturing multicrystalline silicon solar cells (Chen & Wang, 2011), since mc-Si has randomly orientated grains because it is not composed of a single crystal. The most commonly used patterns created through anisotropic texturing of c-Si solar cells are random upright pyramids, regular inverted and upright pyramids (Honsberg, 2012). Regular pyramids have a square base and lateral edges that are equal in length (Baker-Finch & McIntosh, 2010). Both regular inverted and upright pyramids form an array of pyramids that are equal in size and are created by masking the silicon surface by an appropriate patterned resist layer during the etching procedure (selective corrosion). Inverted pyramid textures are created by etching the pyramids down into the silicon surface. (Singh et al., 2001) While random pyramidal textures are included in most commercial monocrystalline silicon solar cells, regular inverted pyramids have been proven to provide lower reflectance. This is because regular inverted pyramids provoke a larger fraction of light to potentially experience triple bounces. (Gjessing, 2012; Baker-Finch & McIntosh, 2010)

The average size of pyramidal structures varies from 1-10 µm, which can be even several times the size of the incident wavelength (Gjessing, 2012). The size of the textures created is important, especially in the context of microscopic pyramidal structures. The created pyramids can be too small and will not have a high facet tilt angle of 54.74°. In other words, the created pyramids will not yield a double-bounce effect and the desired outcome on light absorption will not be achieved (Luque & Hegedus, 2010).

Solution concentration, temperature and etching time must be controlled in order to provide a complete texturing coverage and optimal pyramid morphology and size. As the etching time increases pyramids grow in size and become more regular and more uniformly distributed. (Chen & Wang, 2011; Baker-Finch & McIntosh, 2010) Homogeneity of the structures can also be improved by adding alcohol in the process. (Luque & Hegedus, 2010) Alcohol, such as ethyl glycol, is assumed to ensure etching uniformity due to its carbon content, which enhances the wettability of the silicon surface (Hylton, 2006). For example, if the alkaline solution used is KOH with 5 wt% concentration, the optimal temperature is 80°C and the optimal etching time is 15 minutes. (Luque & Hegedus, 2010).

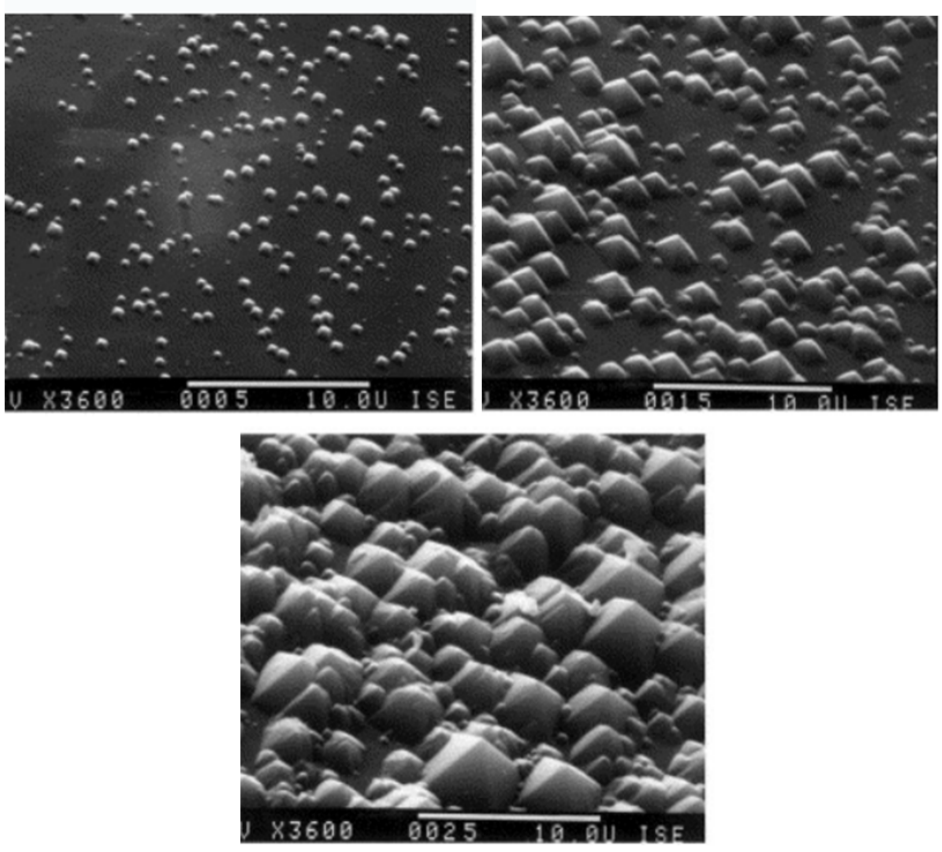


***Figure 3.5.*** *Scanning electron microscope pictures of surface textures after 5 minutes (top left), 15 minutes (top right) and 25 minutes of etching (bottom). (Singh et al., 2001).*

The topography results produced, when a 2 wt% NaOH solution at 80° was used, in a study made by Singh et al. are seen in Figure 3.5. In the study longer etching times,

more than 25-35 minutes, showed that some pyramids started to grow at the expense of others leading to their non-uniform distribution. Thus, optimal surface textures were obtained with an etching time of 25-35 minutes.

If all the etching parameters are optimal and produce desired textures, the front-face reflectance of a c-Si can be significantly reduced. Figure 3.6 shows how reflectance was reduced in crystalline silicon (no ARC) after different etching times with a 2 wt% NaOH solution in the near-bandgap wavelength range.

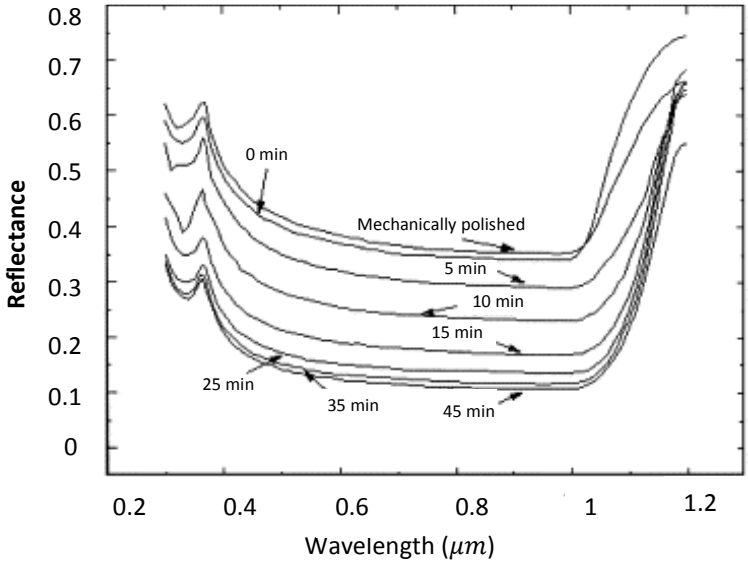


***Figure 3.6.*** *Measured reflectance on anisotropically textured silicon wafer (Singh et al., 2001).*

The graph clearly portrays the benefits of texturing c-Si cells: with the optimal etching time, the reflectance drops to approximately 11-14 % in the wavelength range of 0.45-1 μm, whereas the reflectance of untextured monocrystalline wafer is 35-40 % in the same wavelength range.

Despite the many benefits of alkaline etching of silicon solar cells, it must be emphasized that such technique is only possible for (100) orientated surface planes when pyramids with high antireflection and light trapping properties are required (Bean, 1978). Also, one other disadvantage of anisotropic type of texturing is that it cannot be applied to very thin solar cells that have a thickness typically in the order of a micron. This is because the created pyramids tend to remove a large part of the material (Gjessing, 2012).

### 3.3.2 Texturing multicrystalline silicon solar cells

Multicrystalline silicon mainly consists of randomly orientated grains as opposed to monocrystalline silicon. Only a very small part of the mc-Si surface is covered with (100) orientated planes, which complicates the texturing process of such surfaces with anisotropic etching solutions (NaOH and KOH). (Macdonald, et al., 2004) Nevertheless, it is still possible to create textures on mc-Si solar cell surface through alkaline etching

techniques. However, since there are only few properly orientated grains at the wafer surface that are capable of yielding high angled (54.74°) pyramidal structures when exposed to an anisotropic etch, the rest of the structures will not have a proper orientation and will not achieve the desired decrease in front-surface reflectance. Because of that also the overall light trapping capabilities of the solar cell will be less effective. (Macdonald, et al., 2004; Gjessing, 2012; Hylton et al., 2004) In addition, alkaline solutions may cause unwanted steps and crevasses between the grains, since some grains will require less etching time than others.

The surface of mc-Si after isotropic etching (or acidic etching) tends to consist of a random dimple-like structure (Figure 3.7) as opposed to pyramids with well-defined facet angles on c-Si after anisotropic etching (Figure 3.5).

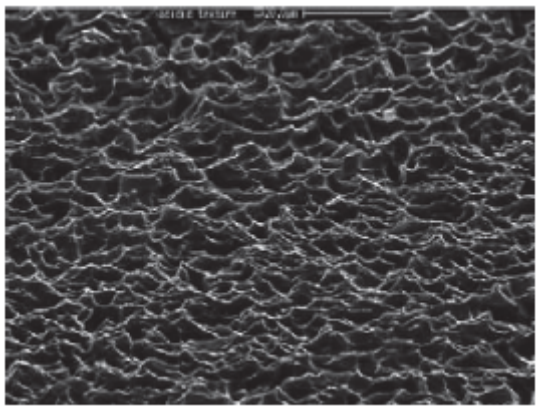

***Figure 3.7.*** *Texture of mc-Si after isotropic etching (Gjessing, 2012).*

Isotropic etchants etch approximately at the same rate and with the same characteristics regardless of the crystallographic direction (Hylton, 2006). Rounded surface features achieved through wet acidic texturing have good antireflection properties. (De Wolf, et al., 2000; Nishimoto et al., 1999) V-shaped grooves can also be produced when employing such etching technique. Essentially, grooves can have an opening angle ranging from 40-120° and they are 2D structures as opposed to pyramids that are 3D structures (Gjessing, 2012).

Masked and maskless reactive ion etching is another promising texturing techniques for multicrystalline cells (Macdonald, et al., 2004). Winderbaum et al. (1997) have shown that the use of ‘dry’ RIE as a texturing technique in conjunction with a mask produces regular features, while Ruby et al. (1999) have shown that maskless RIE texturing techniques produces much smaller and more random textures. Both RIE techniques are capable of producing pyramids and V-shaped grooves. (Winderbaum et al., 1997; Ruby et al., 1999)

Figure 3.8 portrays the results of reflectance of textured multicrystalline silicon surfaces without an ARC in the study made by Meng (2001). It can be seen from the graph that the reflectance after acidic etching is significantly lower than after the other

two texturing techniques, indicating that it is a much more suitable method of texturing mc-Si than the alkaline etching technique.

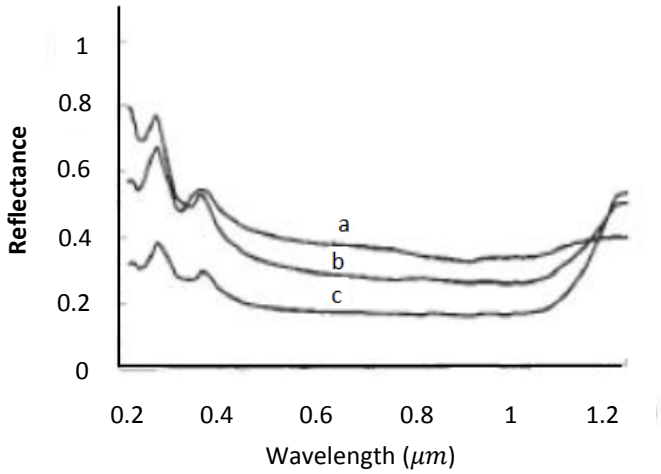


***Figure 3.8.*** *Measured reflectance of a multicrystallline surface: curve a represents alkaline etching (NaOH solution), curve b represents alkaline etching (NaOH) after acidic etching and curve c stands for acidic texturing (Meng, 2001).*

It can be seen from Figure 3.8 that the best results are achieved through isotropic etching (curve c) with reflectance of approximately 20 % in the wavelength range of 0.4-1 µm. However, despite the fact that isotropic etching results in a lower reflection than alkaline etching of mc-Si, the reflectance of textured monocrystalline semiconductors remains approximately 5-10 % lower (Gjessing, 2012; Chen & Wang, 2011).

In a study made by MacDonald et al. (2004) it was shown that some of three texturing methods more suitable for mc-Si (acidic texturing, masked and maskless RIE texturing) proved to be more efficient than others. The reflectance results with no antireflection coating varied from 11 % to 34.4 % in the wavelength range of 0.3-1.2 µm. Masked RIE texturing technique yielded the lowest reflectance of all methods and thus proved to have a greater effect on improving the performance of solar cells. The highest reflectance values were achieved through wet acidic texturing. Nevertheless, it was noticed that the relative difference between methods was reduced after an addition of a SiN antireflection coating. The yielded reflectance values varied only between 4 % and 9 %, depending on the method, in the same wavelength range as mentioned above.

Reactive-ion-etching techniques consequently prove to be considerably more effective in reducing the reflectance of a mc-Si solar cell than alkaline etching and acidic etching techniques, especially when no ARC is present. However, RIE is a relatively expensive type of etching. (Macdonald, et al., 2004)

## 3.4 Disadvantages of surface textures

Textured surfaces create an uneven distribution of the transmitted light by multiple reflections. While this decreases front-face reflection losses and enhances light-trapping

capabilities of the solar cell, it also complicates modeling light-behavior on such surfaces. In other words, estimating the cell's reflectance becomes a more complicated task. Since reflectance plays an important role in the overall performance of the cell, estimating the cell's efficiency becomes more complicated as well (Chen & Wang, 2011; Macdonald, et al., 2004). Also, as mentioned earlier due to an increase in the front surface area of textured silicon, the amount of surface recombinations occurring in textured solar cells is larger than in flat cells (Basore, 1990). However, whether this affects significantly the solar cell performance is described in the next section.

## 3.5 Impacts of texturing on quantum efficiency

Roughening the solar cell surface with optimal etching parameters and thus producing desired textures with significant antireflection and light trapping capabilities has shown to improve the performance of the cell (Basore, 1990). For instance, texturing solar cells yields higher spectral response values. The difference is particularly noticeable in the longer wavelength region. Since quantum efficiency is conceptually similar to spectral response, the QE of a cell is also improved due to texturing.

Surface texturing greatly affects the EQE of the cell. Since EQE involves optical losses caused by front surface reflection, as shown in equation 3.1, lowering the front-face reflection through texturing would increase the EQE.

$$EQE = (1 - \rho) \cdot IQE \tag{3.1}$$

However, since the IQE of the cell already considers photons that were actually able to penetrate the solar cell, it provides a more useful analysis when considering which other effects (both optical and electrical) surface textures have on the solar cell performance. As mentioned, surface recombination velocities and diffusion lengths have impacts on the IQE of the cells. The effect on the conversion efficiency of the front-surface recombination velocity is of particular interest when examining textured cells.

Yang et al. (2008) analyzed how the IQE of a solar cell varied when the emitter surface recombination velocity $S_e$ varied, while other parameters of the cell, such as diffusion length in the emitter region, remained unchanged (Figure 3.9). The total IQE of a cell is the sum of the emitter, space charge and base regions. It can be seen from the graph that the emitter recombination velocity mainly affects the IQE of the cell in the short wavelength region: as front surface recombination velocity is increased, the contribution of the emitter region to $J_{sc}$ is reduced, and thus the total IQE is decreased as well, at the corresponding wavelengths. The contributions of the base and space charge region (depletion region), on the other hand, are not affected by front-surface recombination velocity.

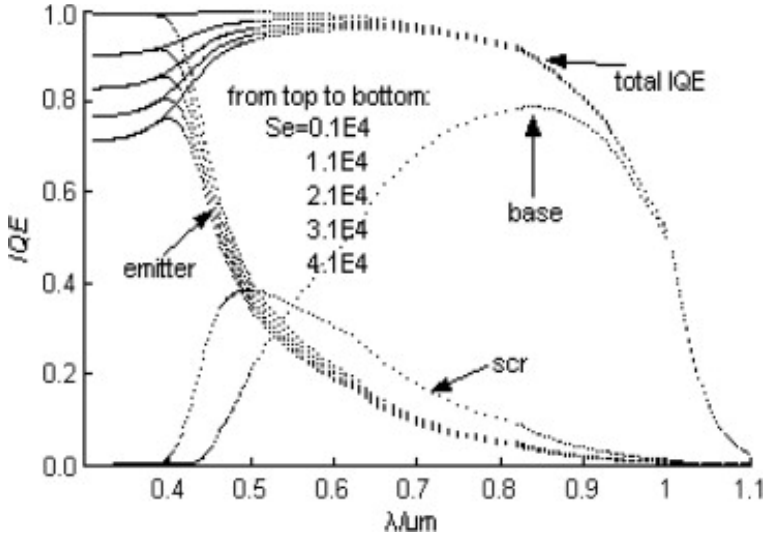


***Figure 3.9.*** *Different front surface recombination velocities of the emitter and their impact on the IQE of the emitter region and the overall IQE of a flat cell (Yang, et al., 2008).*

Furthermore, studies made by Yang et al. (2008) and Basore (1990), where the solar cells considered had no passivation of the surfaces, are in agreement that the IQE of the cell, is mostly dependent on the diffusion length of the base region $L_b$. The diffusion length is an electrical property of the cell that is not affected by surface textures.

Another important parameter to be considered that can deteriorate the performance of non-passivated textured cells is the back surface recombination $S_{bs}$. However, when considering a front-face texturing configuration, the increase of surface area provoking increased surface recombination occurs only in the front surface of the cell. (Reynolds & Meulenberg, 1974) Thus, the back surface recombination velocity is a parameter that is independent of front-face texturing.

When estimating the IQE of a solar cell that is textured, the beneficial effect of path length enhancement of light has to also be taken into account. As mentioned, in a textured cell light travels in a slantwise way (at an angle), therefore it travels a longer path before reaching the back surface, when compared to flat cells. This ensures that lower energy photons are absorbed while still in the base region of the solar cell. Hence, more photons have a chance to be absorbed before reaching the back surface. Texturing a cell can therefore increase the path of light within the cell. This in turn results in higher IQE values at longer wavelengths (Wang et al., 1990). Therefore, with a smaller cell thickness, a textured solar cell can provide the same IQE values as a thicker flat solar cell (Yang et al., 2008). This characteristic of textured cells is particularly important, since the production costs can be minimized. Also, if compared to a flat cell, propagation of normally incident photons at an angle within the textured cell generates more minority carriers in the base region near the depletion zone, having thus shorter lengths to travel before being collected.

In the analysis made by Wang et al. (1990) the passivated emitter, rear locally diffused (PERL) solar cell structure was considered with inverted pyramids as a light trapping and an antireflection method. In such cells, open-circuit voltage $V_{oc}$ and short-circuit current $J_{sc}$ are high due to very low recombination rates in the bulk and in the front and rear surfaces. Due to these characteristics, the IQE of the cell is not influenced much by the diffusion length and surface recombination velocities. In the study the IQE of PERL cell was compared with the cell's hemispherical reflectance. Hemispherical reflectance considers the reflection from the front of the silicon surface, as well as the fraction of photons that managed to penetrate the solar cell but were not absorbed within the cell and have escaped from the front surface. Therefore, hemispherical reflectance is also dependent on $\rho_{bs}$, especially, according to Basore (1990), at longer wavelengths. Back surface reflectance plays an important role when poorly absorbed light reaches the back reflector on the first trip and is reflected to get another chance for absorption. It was shown in the study made by Wang et al. (1990) that improving the rear surface reflectance mainly increases the IQE in the longer wavelength region. This is due to the fact that low energy photons corresponding to long wavelengths are not absorbed in their first route and reach the back surface of the cell. Therefore, it is important that the reflectance of that surface is close to unity; so that all the photons can be reflected and hence have another chance for absorption. Hence, it was noticed that the main mechanism for improving the IQE of a textured cell with low recombination rates in the bulk and in the surface is improving the back surface reflectance $\rho_{bs}$. Naturally, $\rho_{bs}$ is a solar cell parameter that is not affected by surface textures. This observation highlights the importance of passivating the emitter and rear surfaces of the cell: if such surfaces were passivated, the deteriorating effect on the IQE of surface textures is negligible. It was also noted by the authors that the main contributor to the exponentially high $J_{sc}$ is the high IQE (near 100 %) of PERL cells. The reason for that is that virtually every photon absorbed in the silicon by EHP generation contributes to $J_{sc}$. (Wang et al., 1990; Blakers et al., 1989; Green, 1999)

The same significant influence of the back surface reflectance on the internal quantum efficiency was seen in a study made by Brendel et al. (1996) on textured thin film cells. In their study the first configuration included a thin film solar cell with a back surface reflectance of almost unity. It was shown that the IQE started to decrease only at $\lambda{\sim}1\ \mu m$. However, in the second configuration involving another thin film solar cell with a back substrate that absorbs all the photons, and thus $\rho_{bs} = 0$, it was shown that the IQE values started rapidly decreasing already at approximately $\lambda{\sim}0.8\ \mu m$.

Increased internal front-surface reflectance $\rho_{in}$ in textured cells is in theory assumed to have a positive influence on the IQE, since it is capable to increase the fraction of low-energy photons trapped within cell. Internal front-surface reflectance is another parameter that constitutes the hemispherical reflection. As mentioned, this optical parameter can be increased by surface texturing. However, Basore (1990) showed in his study that deteriorating $\rho_{in}$ does not affect the hemispherical reflectance significantly and has negligible influence on the IQE of the cell.

To conclude, it was shown that even without surface passivation, texturing has more beneficial effects than detrimental effects (increased surface recombination velocity) when compared to perfectly flat cells. This is because according to recent studies the IQE of textured cells is mostly dependent on the solar cell parameters that are independent of texturing, such as diffusion length and back surface reflectance (the latter one particularly in PERL cells), not surface recombination velocities. The benefits of texturing on solar cell performance are achieved mostly by improved light harvesting and enhanced path length of light. (Yang et al., 2008)

# 4 RESEARCH METHODS AND MATERIAL

## 4.1 Introduction

This chapter firstly presents modeling approaches of reflection and transmission behaviors of electromagnetic waves on rough surfaces found in literature (Section 4.2). Later, in Section 4.3, the chosen analytical model is described. This section describes in detail how reflectance and transmittance can be calculated for upright pyramids created on c-Si solar cells using the previously mentioned model. The limitations of the model and the influences on the obtained results are also discussed. Lastly, Section 4.4 presents the method for calculating the IQE of a flat and textured solar cell.

## 4.2 Modeling approaches of surface textures

Most of the recent studies that investigate the influence of surface textures on solar cell conversion efficiency are mostly experimental studies (Campbell, 1993; Singh et al., 2001; Hylton et al., 2004; Xi et al., 2004; Gjessing, 2012). In other words, many studies aim to produce several types of textures varying their physical dimensions through different processing parameters, such as temperature, etching time, etc. (mentioned in Sections 3.3.1 and 3.3.2). Afterwards, the light trapping capabilities, quantum efficiency and/or the short-circuit current of the textured cells are measured. This so-called trial and error method provides little resources for the optimization of texture features in order to extract the most benefits of texturing. Due to this reason modeling of textured surfaces must be considered.

As mentioned previously, there are two approaches in studying light behavior on surfaces: the wave optics regime and the geometrical optics regime. Both regimes are capable of predicting the angular distribution of reflected flux as a function of the angle and wavelength of the incident light. Both modeling approaches can also account for the fact that light is reflected several times before it is sent back to the source. (Torrance & Sparrow, 1967)

### Geometrical optics regime

Geometrical optics models are sufficient to understand the optical behavior of solar radiation incident on a textured surface, providing relatively good accuracy of the results. However, geometrical optics regime is only relevant when expecting little dependence of reflectance and other optical properties on the size of the textures. Since geometrical optics regime ignores the wave nature of light it cannot consider diffraction and inter-

ference effects. On the other hand, the size of the structures most commonly produced on crystalline silicon solar cells is larger than the incident wavelength. In such cases diffraction and interference effects can be neglected.

One effective and commonly used numerical technique that simulates light behavior on surface structures is ray tracing. Some of the more popular models used based on this technique are Monte Carlo ray tracing models (stochastic ray tracing) (Arvo et al., 2003). Ray tracing simulations are usually designed to model regular structures. Because of this, reflection and transmission of incident light from regular textures created on monocrystalline silicon, such as regular upright and inverted pyramids, can be well approximated through such simulations. Nevertheless, models based on ray tracing simulations can also be applied to textures created on multicrystalline silicon, since V-shaped grooves tend to have a regular structure as well. In order for the modeling programs to simulate random textures, such as random pyramids created on c-Si surface, they have to be capable of randomizing the positions of rays inside the sample every time they cross the interface. (Rodriguez et al., 1997)

Some studies that were performed to analyze the reflectance of textured surfaces considered such surfaces as rough interfaces. The analyses were carried out relying on the ray tracing simulations and statistical scattering theory. Nevertheless, such approach is also limited to a scale of texture size larger than the wavelength of incident light. (Byun, et al., 2011; Stephens & Cody, 1977)

In the recent years, a number of versatile ray tracing models have been developed for the photovoltaic community, such as SUNRAYS and Raywiz-Solar (Byun, et al., 2011; Trupke et al., 1997). Despite the fact that ray tracing programs accurately model light behavior on textured surfaces, they are typically computer intensive methods. For this reason an analytical approach to such problems is an alternative. An analytical model based on geometrical optics assumes that each of the pyramid facets is optically flat and reflects specularly. The reflectance and transmittance values can thus be obtained by applying Fresnel's law. In fact, this type of analysis was used in this thesis (see Section 4.3).

### Wave optics regime

When it comes to modeling surface textures that have physical dimensions, which are smaller or in the same order of magnitude as the incident wavelength, the solutions provided by geometrical optics regime no longer provide adequate accuracy. Since physical optics uses a complete physical description of the reflection process, it allows to consider diffraction and interference effects.

Reflectance and transmittance can be estimated by referring to rigorous numerical modeling techniques that solve Maxwell equations. Such numerical modeling techniques are, for instance, finite element method (FEM), finite time domain method (FTDM) and boundary element method (BEM). Just like in the case of ray tracing simulations in geometrical optics regime, these models are computationally intensive and are

thus used in cases when analytical models cannot be employed or when the accuracy of the results provided by analytical models is not satisfactory. (Basore, 1990; He et al., 1991; Clugston & Basore, 1997)

### Challenges

Regardless of the approach or regime employed, random pyramidal textures complicate the analysis in all cases (Baker-Finch & McIntosh, 2010). Since random surface textures are formed by an array of pyramids that vary randomly in size, it is rather difficult to analyze these random conditions precisely. There is, in fact, a chance that light will bounce off the sidewalls of other pyramids, rather than from those pyramids that are opposite (Figure 4.1).

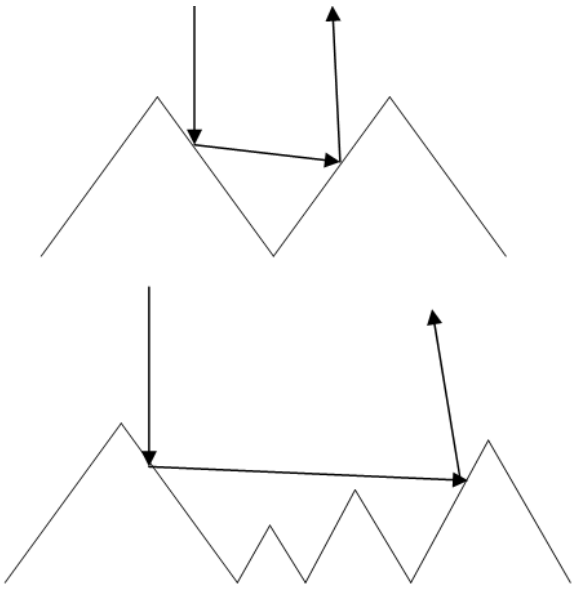

***Figure 4.1.*** *Light bouncing off from the opposite pyramid in regular upright pyramid structure (top) and light not bouncing off from the opposite pyramid (bottom) in random pyramid structure.*

Another factor that complicates the analysis of random pyramids is the fact that light can experience up to 5 bounces from such textures before returning to the source. Nevertheless, several studies are in agreement that the reflectance and transmittance results obtained when approximating random pyramids as regular pyramids do not differ considerably. (Zhao & Green, 1991; Baker-Finch & McIntosh, 2010)

Another challenge of modeling textured silicon solar cells is the fact that more reliable results are achieved when all three dimensions (3D) are considered. On the other hand, considering all the multidimensional effects of textures makes it harder to model the problem analytically, which highlights the benefits and importance of employing numerical methods when more accurate results are required. However, it was pointed out by several studies that some textures can still be well approximated in one-dimension (1D) and two-dimensions (2D) (Baker-Finch & McIntosh, 2010; Brendel et

al., 1996). Yet, it is important to emphasize that even the most sophisticated models can provide inaccurate reflectance and transmittance results due to an indirect or an approximated method that is not able to account for a fully realistic optical environment (Byun, et al., 2011).

## 4.3 Baker-Finch and McIntosh model

### 4.3.1 Assumptions

This geometrical optics model is used in this thesis to estimate the reflectance and transmittance of regular upright pyramids. It is assumed that no matter what the etching technique was, its etching parameters, for instance, solution temperature and etching time, were optimal in order to provide upright pyramidal textures that have high facet tilt angles of 54.74°, thus guarantying good antireflection qualities. Also, it is assumed that there is a uniform and dense coverage of pyramids. More specifically, there are no flat surface areas in between the pyramids, as it is shown in Figure 3.4. The structure size is also assumed to be larger than the wavelength of incident light. As mentioned, the size of the pyramids is typically in the order of 1-10 μm, which is indeed larger than most of the near-bandgap wavelengths. Based on these assumptions, it becomes evident that most likely the etching method used in order to create textures with such properties and morphologies is alkaline etching, which favors the monocrystalline silicon surfaces (Bressers et al., 1996).

Another assumption made is the fact that light illuminating the solar cell is considered to be collimated, despite the fact that typically surfaces are submitted to both collimated and diffuse solar irradiation. Furthermore, reflection from an individual pyramid facet is not considered to be diffuse. In other words, the incident light is assumed to be reflected at a single angle (specular reflection) rather than many angles. Also, in order to maintain the analysis relatively simple, it is assumed that there is no antireflection coating and no encapsulation and/or glass substrate on the surface of the textured silicon. Thus, light is considered to travel directly from the surrounding air into the silicon.

### 4.3.2 Description of the model

The model which the analysis is based on uses a rather simplistic geometrical approach. In a study made by Baker–Finch and McIntosh (2010) the reflection paths and the fraction of rays that follow these paths were determined. Based on this knowledge the front-face reflectance and transmittance of silicon solar cells textured with regular upright pyramids was calculated.

Analyzing solar cell performance under normally incident light provides the most useful reference. This is due to the fact that currently, the majority of solar cell and module testing as well as optimizing studies consider the normally incident light conditions. Nevertheless, the same approach in analyzing reflectance and transmittance of

solar cells can be applied to any incident angle. (Baker-Finch & McIntosh, 2010) When referring to a normally incident light, light is considered to be normal to the silicon interface, and it is thus, not normal on the individual pyramid facet. As demonstrated in Figure 4.2, light that is normally incident in respect to the interface forms an incident angle that is equal to the facet angle of the pyramid.

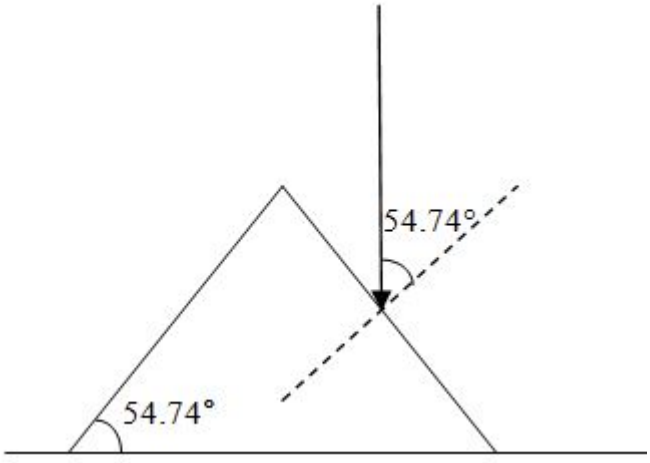


***Figure 4.2.*** *Light incident on an upright pyramid facet at a 54.74° incident angle.*

When light strikes a textured surface, according to Baker-Finch and McIntosh model, regular upright pyramids can exhibit only two possible light paths as illustrated in Figure 4.3 (on the left): path A and path B. If the light is incident on an individual pyramid in the shaded area as shown in Figure 4.3 (on the right), it will undergo three bounces following reflection path B. Light will undergo only two bounces, when following reflection path A, represented as the white area in Figure 4.3 (on the right side).

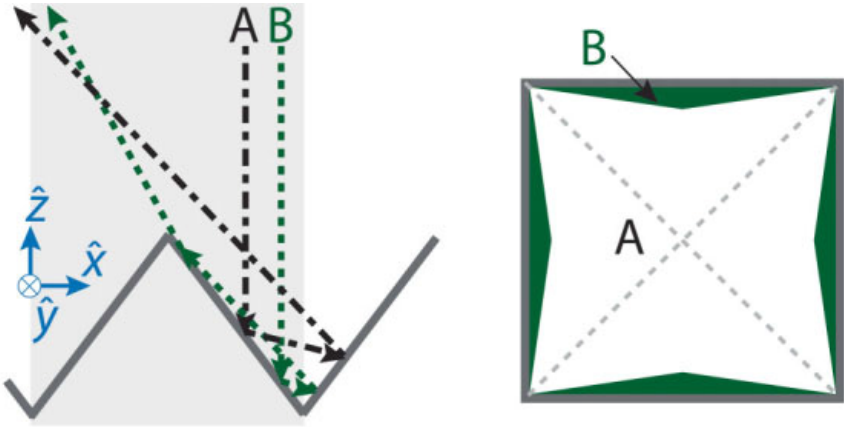


***Figure 4.3.*** *Regular upright pyramidal structures and different paths of light when incident on a pyramid facet (left). View from the top of the pyramid (right) representing the areas that correspond to different paths of light. (Baker-Finch & McIntosh, 2010).*

As it is seen from Figure 4.3, in this model light behavior is analyzed in 2D global coordinates, $\hat{x}$ and $\hat{z}$, where $\hat{y} = 0$. The paths, A and B, were determined experimentally

by baker-Finch and McIntosh (2010) by following the rays reflected from the surface textures.

The reflection paths are determined by the angles at which the incident light is reflected from the facet. The second and the third incident angles can be calculated. Figure 4.4 is an illustration of the incident angles for path A and path B, where $\theta_1 = 54.74°$, $\theta_2 = 15.79°$ and $\theta_3 = 86.32°$.

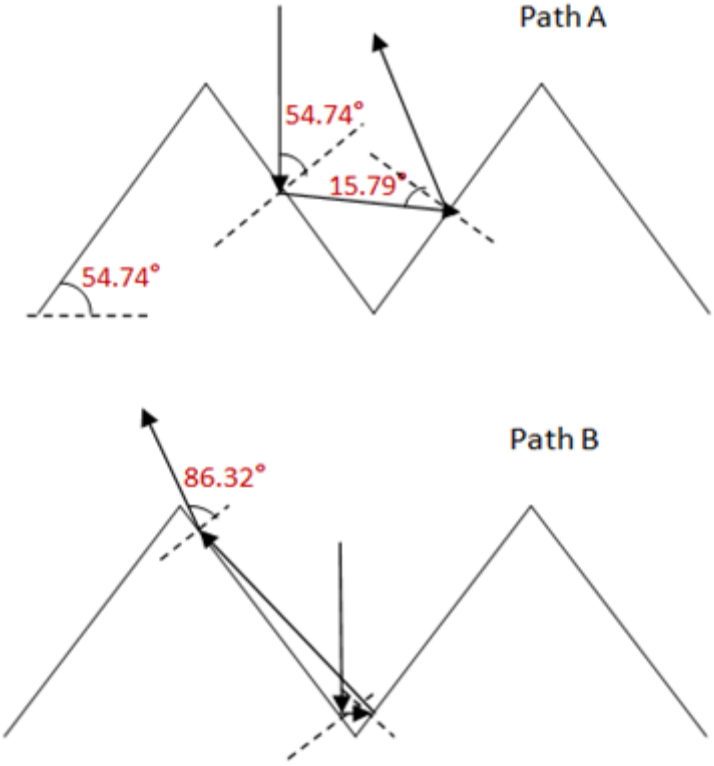


***Figure 4.4.*** *Incident angles at the air/silicon interface of regular upright pyramids for incident light following path A (top) and path B (bottom). The first two angles of incidence for path B are exactly the same as in the case of path A.*

It can be seen that in the case of path B after the second bounce the incident angle is relatively large. As described already in Section 2.4.1, total internal reflection is not possible at the air/silicon interface due to the refractive index of silicon being always larger than the refractive index of air. However, it was mentioned in the same section that when the incidence angle is large, the reflectance also has a relatively large value, signifying that a great portion of light escapes into the air. It should be noted that if a reflection analysis is performed considering, for instance, an encapsulation/silicon interface, total internal reflection is possible at the third bounce (Baker-Finch & McIntosh, 2010). In such cases the third bounce of path B can be ignored, thus path B will become identical to path A.

A so-called probability factor determines the likelihood of an incident ray of light following either path A or path B. The probability coefficients $f_A$ and $f_B$ were determined in the reference study by surface geometry using the area proportions. In the case of only two possible paths for light to choose to follow from, the weighting factors

$f_A$ and $f_B$ are complementary in respect to each other: their sum is equal to unity. (Baker-Finch & McIntosh, 2010)

As it was mentioned earlier the pyramid textures are modeled in a Cartesian basis $(\hat{x}, \hat{y}, \hat{z})$. However, reflectance and transmittance are both evaluated in surface local coordinates $(\hat{s}, \hat{p}, k)$, where $\hat{s}$ is perpendicular to the surface plane (perpendicular polarization state), $\hat{p}$ is parallel to the incidence plane (parallel polarization state) and $\hat{k}$ is parallel to the direction of ray propagation as illustrated in Figure 4.5.

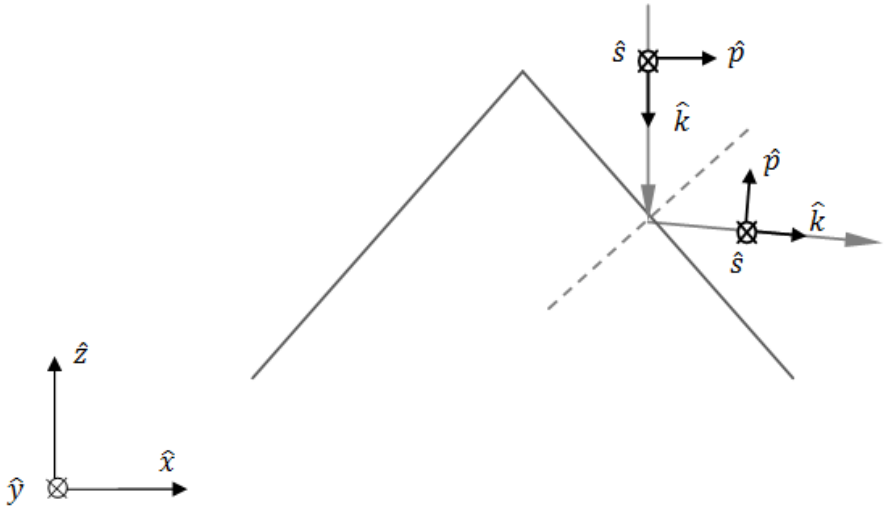


***Figure 4.5.*** *Global and local coordinate systems of regular upright pyramid texture before and after reflection.*

The transmitted angles can be calculated in surface local coordinates using Snell's law described in Chapter 2. Nonetheless, from the point of view of solar cell performance analysis, it is more useful to determine the transmitted angles with respect to global coordinates. A simple geometrical analysis was done in order to obtain the desired angles. Figure 4.6 portrays that in order to calculate the transmitted angle of the first bounce in global coordinates $\theta_{1tg}$ the transmitted angle in local coordinates $\theta_{1t}$ has to be subtracted from the incident angle $\theta_1$.

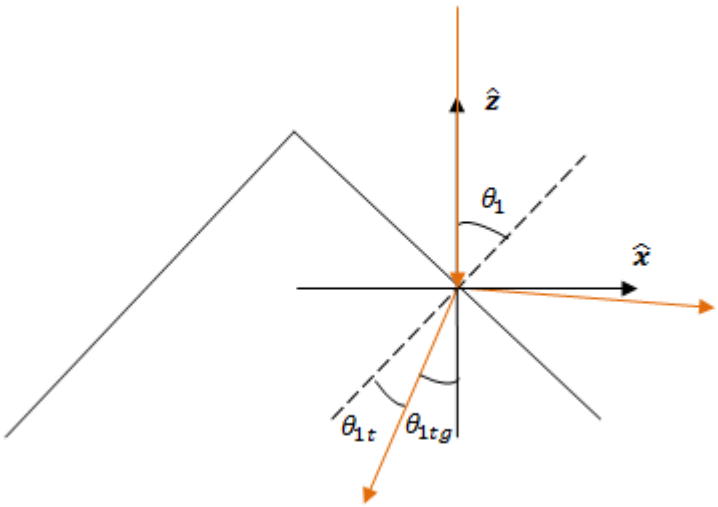


***Figure 4.6.*** *Refracted angle $\theta_{1tg}$ from the first bounce in terms of global coordinates.*

On the other hand, for the second bounce, the transmitted angle $\theta_{2t}$ has to be added to the incident angle $\theta_1$, as shown in Figure 4.7.

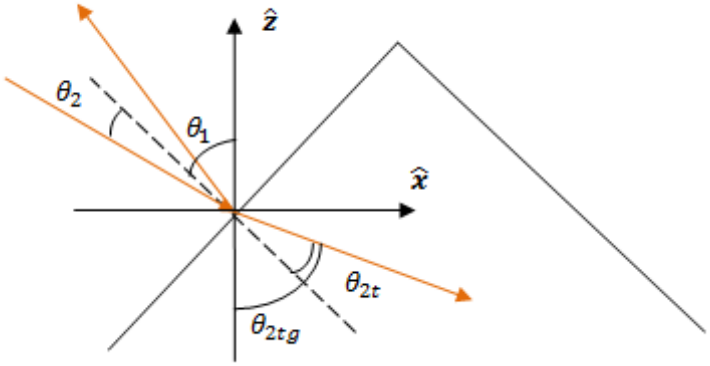


***Figure 4.7.*** *Refracted angle $\theta_{2tg}$ from the second bounce in terms of global coordinates.*

Similarly, in order to get the transmitted angle in global coordinates at the third bounce $\theta_{3tg}$ the transmitted angle in local coordinates $\theta_{3t}$ must be added to the incident angle $\theta_1$, as shown in Figure 4.8.

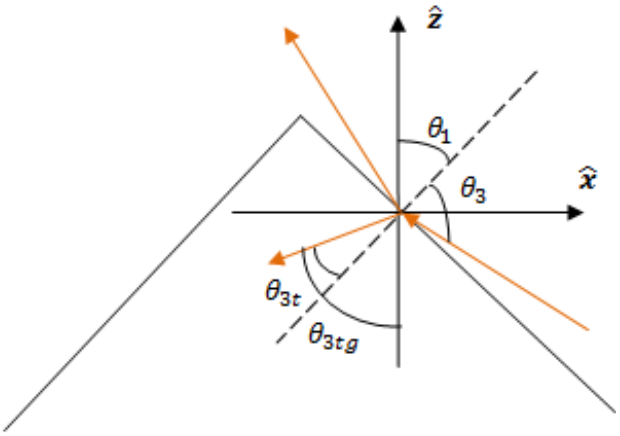


***Figure 4.8.*** *Refracted angle $\theta_{3tg}$ from the third bounce in terms of global coordinates.*

The following equations (4.1-4.3) specify how the desired refracted angles were calculated at each bounce.

$$\theta_{1t,g} = \theta_1 - \theta_{1t} \tag{4.1}$$

$$\theta_{2t,g} = \theta_1 + \theta_{2t} \tag{4.2}$$

$$\theta_{3t,g} = \theta_1 + \theta_{3t} \tag{4.3}$$

### 4.3.3 Reflected flux of regular upright pyramids

Whenever light strikes an interface, a pyramid facet in the cases of this analysis, a fraction of it is reflected $I_{r,j}$ and a fraction is transmitted $I_{t,j}$, where $j$ is the number of bounces that light has undergone, as demonstrated in Figure 4.9.

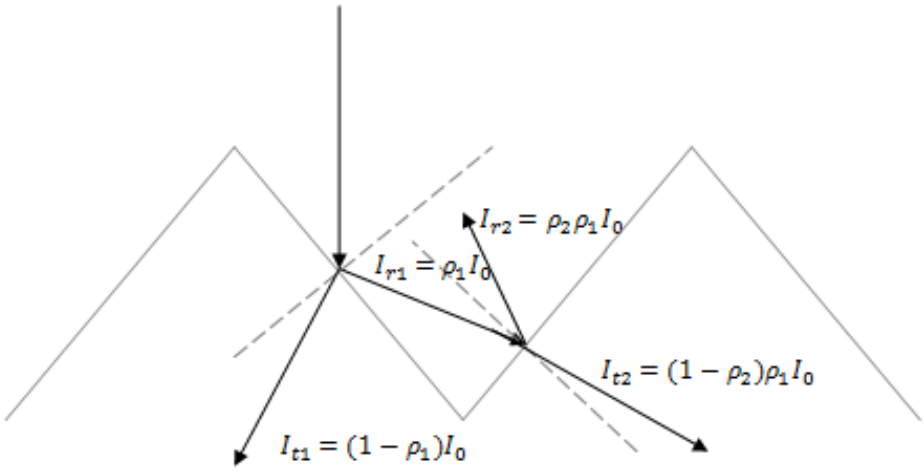


***Figure 4.9.*** *Reflected and transmitted incident solar flux of regular upright pyramids when the light is assumed to follow path A.*

The general formula for the reflected flux of light following a certain path is

$$I_{r,i} = \rho_j \cdot \rho_{j-1} \cdot \rho_{j-2} \cdot \ldots \cdot \rho_1 I_0 \tag{4.4}$$

where $i$ represents either path A or path B. The number of paths in pyramidal structures can vary. For, example for regular inverted pyramids (analysis in 3D), the authors of the model determined three distinct paths, and for random pyramids the number of different paths was up to seven. However, since in this work only the case of upright pyramids is considered and analyzed in 2D, there are only two distinct paths.

The reflected flux for path A is

$$I_{r,A} = \rho_2 \rho_1 I_0 \tag{4.5}$$

where $I_0$ is the incident flux expressed in $\frac{W}{m^2}$ and $\rho_1$ and $\rho_2$ are reflectances of the first and second bounce. Similarly, the reflected flux from path B is

$$I_{r,B} = \rho_3 \rho_2 \rho_1 I_0 \tag{4.6}$$

where $\rho_3$ is the reflectance of the third bounce.

According to this model the total reflected flux of a pyramidal structure is defined as a weighted sum of individual reflected fluxes $I_{r,i}$ that follow certain paths, represented in the following equation.

$$I_{R,reg,up} = \sum_{i=A,B} f_i \, I_{r,i} \tag{4.7}$$

The total reflected flux $I_{R,reg,up}$ of upright pyramids is thus, the summation of the product of different reflectances corresponding to a certain path and the associated weighting factors $f_i$. Equation can thus be expressed as

$$I_{R,reg,up} = f_A I_{r,A} + f_B I_{r,B} = 0.8889 I_{r,A} + 0.1111 I_{r,B} \tag{4.8}$$

where the reflectance of path A and path B are added together each of them assigned to a weighting coefficient, $f_A = 0.8889$ and $f_B = 0.1111$ respectively. Equation 4.8 can be expressed in terms of reflectances with the following equation.

$$I_{R,reg,up} = 0.8889 \rho_2 \rho_1 I_0 + 0.1111 \rho_3 \rho_2 \rho_1 I_0 \tag{4.9}$$

As mentioned previously the reflectance at the third bounce $\rho_3$ due to the large incident angle, can be quite large. In such cases, the assumption that $I_{r,B} \simeq I_{r,A}$, can be allowed. Therefore, the reflected flux of regular upright pyramid is

$$I_{T,reg,up} \simeq I_{t,A} \tag{4.10}$$

However, in this study, in order to obtain more accurate results, the third bounce was taken into account, despite the fact that the reflectance of that bounce was large.

### 4.3.4 Transmitted flux of regular upright pyramids

Equation 2.16 that describes the energy conservation law at the interface presented in Section 2.4.2 and also portrayed in Figure 4.9 was used to estimate the transmitted flux $I_{t,j}$ at each interaction of light and a pyramid facet. However, it is also essential to point out, that when assuming an ARC on the silicon substrate, there is some absorption in the interface and the energy conservation law cannot be directly applied in such cases. Thus, the general expression for the transmitted flux following path $i$ is

$$I_{t,i} = (1-\rho_1)I_0 + \sum_{j=2}^{m}\left(1-\rho_j\right)\left(\prod_{k=1}^{j-1}\rho_k\right) \tag{4.11}$$

where $m$ is the number of bounces the light can undergo in total when following a certain path: two when light is following path A and three when following path B in regular upright pyramids. Thus, equation 4.11 can be reformulated as equation 4.12 and equation 4.13, each representing the transmitted flux of light following path A and path B respectively.

$$I_{t,A} = (1-\rho_1)I_0 + (1-\rho_2)\rho_1 I_0 \tag{4.12}$$

$$I_{t,B} = (1-\rho_1)I_0 + (1-\rho_2)\rho_1 I_0 + (1-\rho_3)\rho_2\rho_1 I_0 \tag{4.13}$$

From the above equations and Figure 4.9 it can be seen that there is a total of five transmitted rays, and in order to obtain the total transmitted flux, all the individual transmissions must be summed with the associated weightings as follows

$$I_{T,reg,up} = 0{,}8889 I_{t,A} + 0{,}1111 I_{t,B} \tag{4.14}$$

In the case of reflected flux, at the third bounce of path B, the reflectance can in some cases be equal to unity, which results in no light being transmitted at this bounce, thus $I_{t,B} \simeq I_{t,A}$ and

$$I_{t,red,up} \simeq I_{t,A} \tag{4.15}$$

Nevertheless, as mentioned earlier, the third bounce of path B is taken into account in this analysis.

### 4.3.5 Limitations of the model

Geometrical optical modeling is limited to analyzing textures with sizes that are much larger than the wavelength of incident light, since this type of modeling does not ac-

count for diffraction and interference effects. Another limitation of the model is the fact that it cannot be applied to a random array of upright pyramids (pyramids that differ in size), otherwise referred to as random pyramids. This limitation is rather important, since random pyramid textures are most commonly featured in solar cell texturing and in high-efficiency solar cells. However, with the help of 3D ray tracing calculus as a complementary method to this analysis, reflection and transmission of random pyramids can be obtained.

Another limitation of the model is the fact that some studies are in disagreement whether incident light can experience a triple bounce on regular upright pyramids. The authors of the model state that regular upright pyramids can in fact yield a triple bounce with a 11 % probability (weighting coefficient $f_B$) (Baker-Finch & McIntosh, 2010). Meanwhile, Smith et al. (1993) state that no rays can experience a triple bounce when striking upright pyramid geometries. Both studies however, agree that approximately 40 % of the incoming light is likely to experience a triple bounce on the surface of inverted pyramids. Yet, the analysis in this thesis focuses only on regular upright pyramids and thus, the inconsistency of observations related to upright pyramid texture may affect the reliability of the results when using the Baker-Finch and McIntosh model.

## 4.4 Internal quantum efficiency analysis

As mentioned earlier, in order to analyze the total IQE of a solar cell, contributions from all cell regions have to be taken into account, as follows

$$IQE_{total}(\alpha) = IQE_e(\alpha) + IQE_{scr}(\alpha) + IQE_b(\alpha) \tag{4.16}$$

where internal quantum efficiency is expressed as a function of absorption coefficient $\alpha$, which is in turn wavelength dependent (Yang et al., 2008). Nevertheless, the total IQE of solar cell can be well approximated when considering the contributions to the total IQE only in the bulk region. In other words, in this case the cell is assumed to have a large penetration depth compared to the thickness of the emitter $w_e$ and space charge region $w_{scr}$ ($w = w_e + w_{scr} \ll \alpha^{-1}$). In the red and throughout the near-IR spectral range, i.e. in the range of 0.6 -1.2 μm, a following equation governs the IQE of a flat silicon solar cell

$$IQE_{total}(\alpha) \approx IQE_b(\alpha) = \frac{\alpha \cdot L_b}{\alpha \cdot L_b + 1} \tag{4.17}$$

Neglecting the contributions to the total IQE of the emitter and space charge regions introduces slight errors in the short wavelength range, mainly when $\lambda < 0.5\ \mu m$. This is due to the fact that the contributions of the emitter and the space charge region are more significant particularly in that wavelength region. (Basore, 1990; Bücher et al., 1994; Yang et al., 2008; Terman, 1961) However, since the error introduced by this assumption is relatively small and mainly concerns a small fraction of the wavelength region

used in the analysis part of this thesis (Chapter 5), equation 4.17 was employed to estimate the total IQE of a flat cell.

The total IQE of a textured cell according to Yang et al. (2008) can be calculated as follows

$$IQE_{total}^{textured}(\alpha) = \frac{L_b \cdot \alpha / \cos(\theta_{1tg}) + 1 - e^{-\alpha \cdot w / \cos(\theta_{1t})}}{L_b \cdot \alpha / \cos(\theta_{1tg}) + 1} \tag{4.18}$$

It can be seen that the transmitted angles in both global and local coordinates of the first bounce are required.

Only the front surface reflectance of a solar cell was analyzed in this thesis. Equations 4.17 and 4.18 that govern the total IQE of a flat and textured cell are thus, more suitable. This is due to the fact that these equations require the cell thickness $H$ to be large compared to the light penetration depth ($H \gg \alpha^{-1}$), which signifies that all light is expected to be absorbed before reaching the back surface of a cell. This in turn implies that $\rho_{in}$ and $\rho_{bs}$ can be ignored from the equations of the total internal quantum efficiency of a cell.

# 5 RESULTS AND DISCUSSION

## 5.1 Introduction

A short code was developed in order to simulate light behavior on regular upright pyramids (Appendix A). The simulation code is based on the chosen modeling type of reflection on textured surfaces described in Chapter 4. The goal of the code is to calculate the overall transmitted and reflected flux of regular upright pyramids. The code also simulates for comparison the reflectance and transmittance of a perfectly smooth silicon surface, as well as the reflectance of a bare silicon surface covered with a single layer $SiO_2$ ARC. Section 5.2 presents the results of reflectance and transmittance of regular upright pyramids. Section 5.3 presents the results of the QE analysis performed on textured solar cells with reduced reflectance. The analysis is based on the equations governing the IQE of a flat and textured cell introduced in Chapter 4. The goal of this section is to portray mainly how reduced reflectance affects the EQE and IQE of the cell. Lastly, Section 5.4 covers the discussion related to the analyses performed in this thesis as well as some open issues, and Section 5.5 presents suggestions for future work.

## 5.2 Reflectance and transmittance results

The analysis was performed in the 0.285-1.195 μm wavelength range, since on this particular wavelength range photogeneration takes place, and also the refractive index of silicon varies significantly (see Figure 2.10). Figure 5.1 shows the distribution of transmitted angles at first, second and third bounces in respect with $\hat{z}$ –axis (in global coordinates). One important factor to consider is the fact that $\theta_{2tg}$ and $\theta_{3tg}$ are relatively large. As a consequence, the refracted beam of light might not propagate directly into the bulk of the silicon to produce an electron-hole pair. Instead, it can potentially strike the opposite facet of the same pyramid, as shown in Figure 5.2.

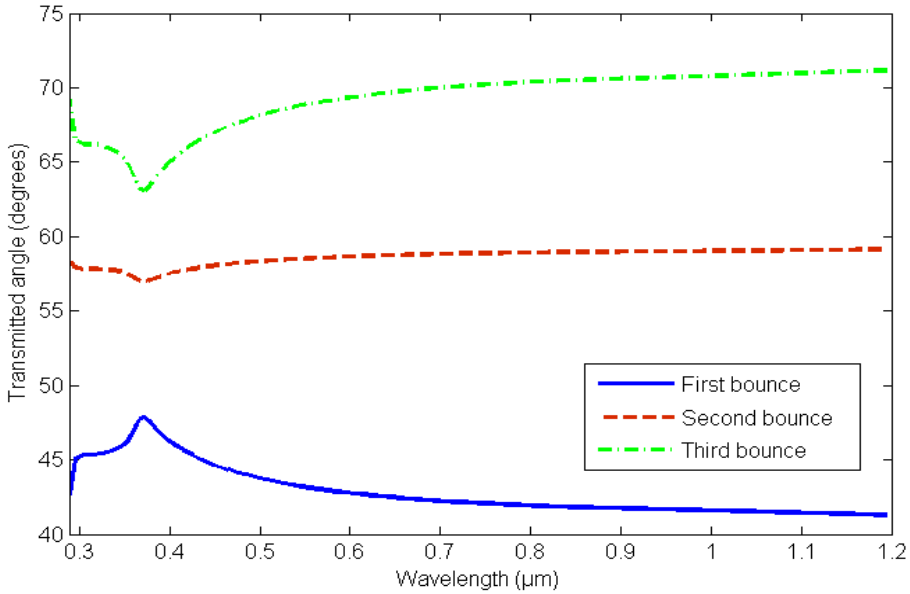


***Figure 5.1.*** *Transmitted angles in $(\hat{x}, \hat{y}, \hat{z})$ coordinates at the first, second and third bounces of a silicon surface textured with regular upright pyramids.*

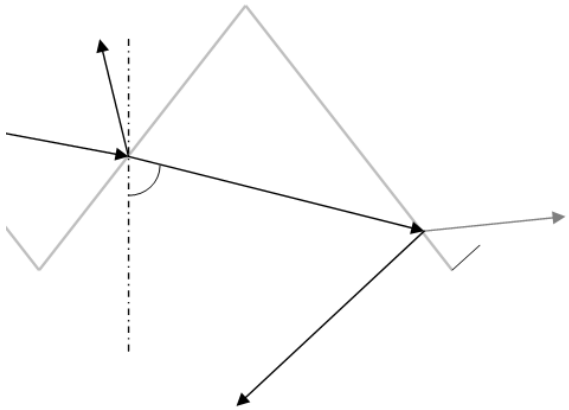

***Figure 5.2.*** *Transmitted light striking the opposite facet of the same pyramid. A fraction of that is then reflected to propagate into the bulk of the silicon and to be absorbed.*

In such scenario only the reflected fraction of light from the opposite facet of the same pyramid will be absorbed. This results in lower transmittance since a certain fraction of that light will escape back into the air. However, from Figure 5.1, it can be seen that on the second bounce the transmitted angles in global coordinates are only slightly larger than the facet tilt angle of the pyramid, 54.74°. This signifies that only a small fraction of rays, that are incident next to the top of the pyramid, will not propagate directly into silicon material. As a consequence, it can be assumed that all light propagates directly into the bulk at the second bounce. At the third bounce on the other hand, the angle of transmission is much larger than the facet tilt angle signifying that a much larger fraction of light might undergo the behavior described in Figure 5.2. However, in order to

assess whether this needs to be taken into, it is useful to look at how much power is transmitted at the third bounce, which is illustrated in Figure 5.3.

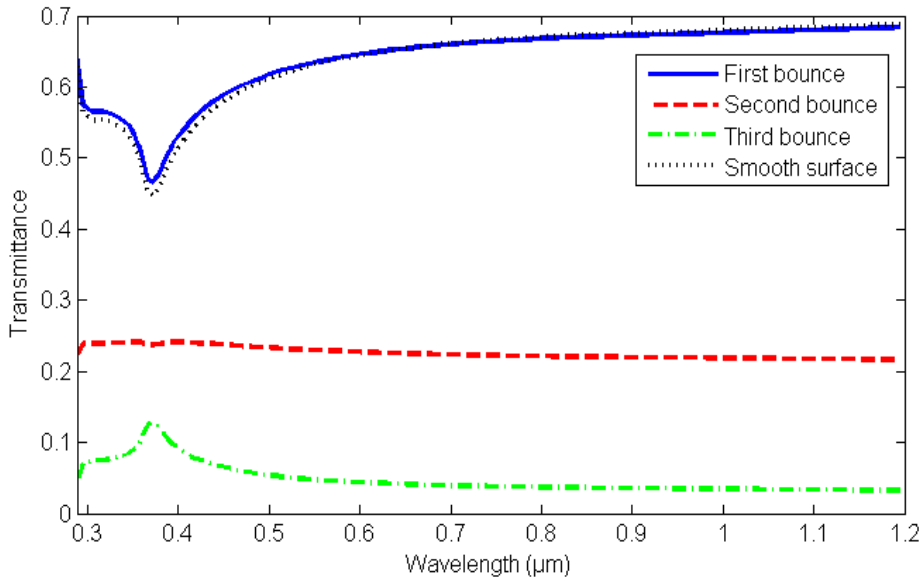


***Figure 5.3.*** *Transmittance at the first, second and third bounces of a surface textured with regular upright pyramids, and the transmittance of a perfectly smooth surface.*

The beneficial effect of textured surfaces due to multiple bounces on the overall front-surface transmittance can be seen right away from the graph. In addition, the transmittances of the first bounce and a perfectly flat surface tend to slowly increase as the wavelength increases, reaching a nearly constant value. This is because the refractive index remains constant at such wavelengths as well. Nevertheless, it can be seen from Figure 5.3 that the transmittance at the second and third bounces tends to decrease as the wavelength increases, also reaching a nearly constant value. This happens because as the wavelength increases, more flux is transmitted at the first bounce, hence less is transmitted at the second and third bounces since the amount of light reflected after the first bounce is reduced.

Figure 5.3 shows that the values of transmittance approach 68 % as the wavelength increases for both bare silicon surface and the first bounce on upright regular pyramids. At the second bounce transmittance decreases considerably to approximately 21 %. This value seems reasonable since only 32 % of the initial flux is reflected onto the opposite pyramid facet. Finally, only 3 % of the initial incident light is transmitted at the third bounce. The ratio between the transmitted and reflected fractions from the second pyramid facet at the third bounce is around 27 %. Such low transmission originates from a very large incident angle at the third bounce, 86.32°. Essentially, even though there is no total internal reflection, a very large fraction of light is indeed reflected from the third bounce. This means that an assumption can be made that transmitted light at the third bounce makes no detour as described in Figure 5.2, since only 3 % of the initially incident light is transmitted at this bounce. Also, as mentioned previously, a

third bounce can only occur with a probability of 11 %, implying that in reality only 0.33 % of the initial incident light on the solar cell is transmitted at the third bounce.

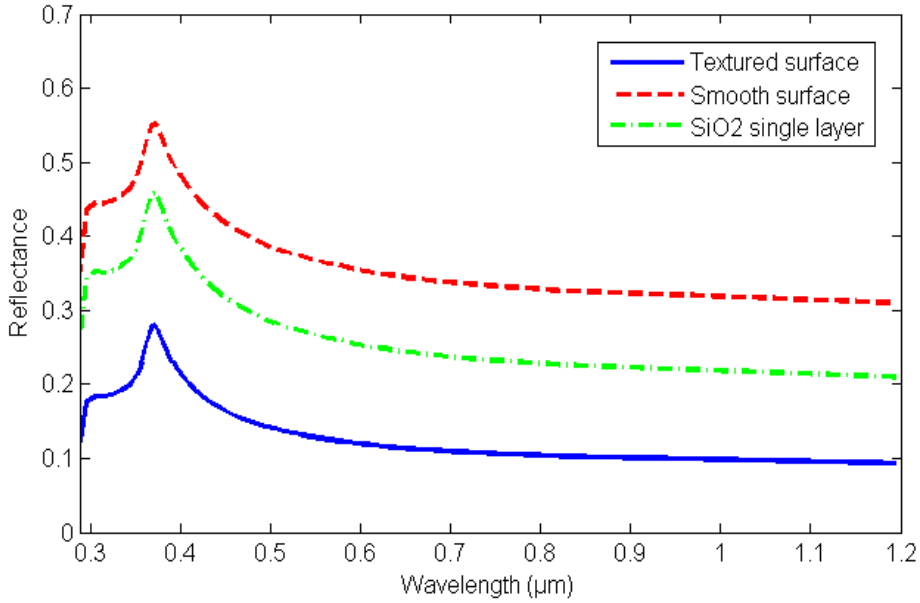


***Figure 5.4.*** *Reflectance of a perfectly smooth surface, a textured surface with upright pyramids, and a single-layer $SiO_2$ ARC.*

Figure 5.4 demonstrates reflectance from regular upright pyramids in comparison with the reflectance of a smooth surface and the reflectance of a single layer ARC of $SiO_2$ on bare silicon. The reflectance of bare silicon reaches a constant value of ~31 % at longer wavelengths. On the other hand, reflectance of a silicon substrate with a $SiO_2$ single layer ARC approaches the value of ~21 %. At the same time, the reflectance of a textured surface reaches a constant value of only ~10 %. There seems to be a decrease of approximately 21 % of the overall reflectance between the textured and bare silicon surfaces. These results highlight the importance of using textured surfaces to improve light harvesting due to smaller front-face reflection losses.

Finally, Figure 5.5 represents the amount of transmitted flux from a textured surface in comparison with the amount of transmitted flux with a perfectly smooth surface and the incident solar flux at AM1.5 spectrum as a function of wavelength. The yellow area represents the flux that can be gained when texturing silicon solar cells with regular upright pyramids.

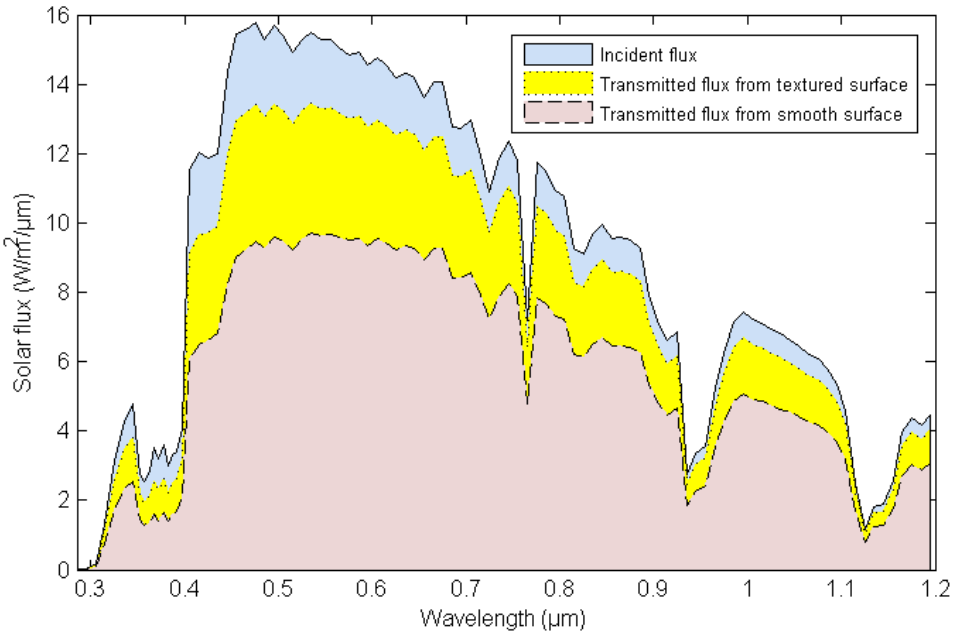


***Figure 5.5.*** *AM1.5 incident solar flux and the fractions of it that are transmitted from textured and flat surfaces.*

The incident solar flux at AM1.5 spectrum is given as integrals between two distinct wavelength values over wavelength range of 0.285-1.195 µm. Thus, Figure 5.5 represents a single value of incident solar flux as a function of an average wavelength value between two limits of each interval.

In the results of the experimental study made by Singh et al. (discussed in Section 3.3.1), the reflectance of a monocrystalline silicon solar cell within the wavelength range of 0.4-1.0 µm was ~11 % after 25-35 minutes of etching time with a 2 wt% NaOH based solution with no antireflection coating. The etching conditions imply that fully developed pyramidal structures, such as regular upright pyramids, uniformly cover the silicon surface, which is consistent with the assumptions made in the analysis of this thesis. The measured front-surface reflectance value by Singh et al. (2001) seems to be rather close to the ~10 % result obtained in this analysis.

In a study made by Baker-Finch and McIntosh the reflectance of regular upright pyramids was only ~2 %. The difference between the reflectance values obtained by the authors of the model and by the analysis in this thesis mainly originates from the fact that Baker-Finch and McIntosh assumed there was an ARC coating and an encapsulant on the silicon substrate. The refractive indices of the encapsulant and the ARC coating, as well as its thickness, play an important role when determining the reflectance of a solar cell (Fonash, 2010). Even though encapsulation of silicon does not provide significant results in improving silicon's optical properties to the same extent as the surface textures or ARC do, it nevertheless results in enhanced light trapping. As described earlier, light that is reflected from the back surface can undergo total internal reflection at

the glass/air interface receiving a second chance to enter the cell. Therefore, the very low value of reflectance result calculated by Baker-Finch and McIntosh (2010) is due to a combination of three antireflection and light trapping methods: surface textures, ARC and encapsulation.

Lastly, the obtained results were compared with a study made by Meng (2001) mentioned in Section 3.3.2. In their study the reflectance of a textured multicrystalline silicon substrate with an isotropic etching technique was approximately 20 %. The results seem reasonable since texturing multicrystalline silicon even with the appropriate texturing method, acidic etching in their case, results in higher reflectance due to non-ideal texture morphology and coverage, than alkaline texturing of monocrystalline silicon.

## 5.3 Quantum efficiency results

In this section the results of the IQE and EQE of a flat and textured cell are shown. The analysis is based on the equations presented in Section 4.4. It was assumed that $w_e = 0.5\ \mu m$, $w_{scr} = 1.0\ \mu m$ and $L_b = 100\ \mu m$. The results are presented in the same spectral range as the results in the previous section. Figure 5.6 portrays the IQE values of a textured and flat solar cell.

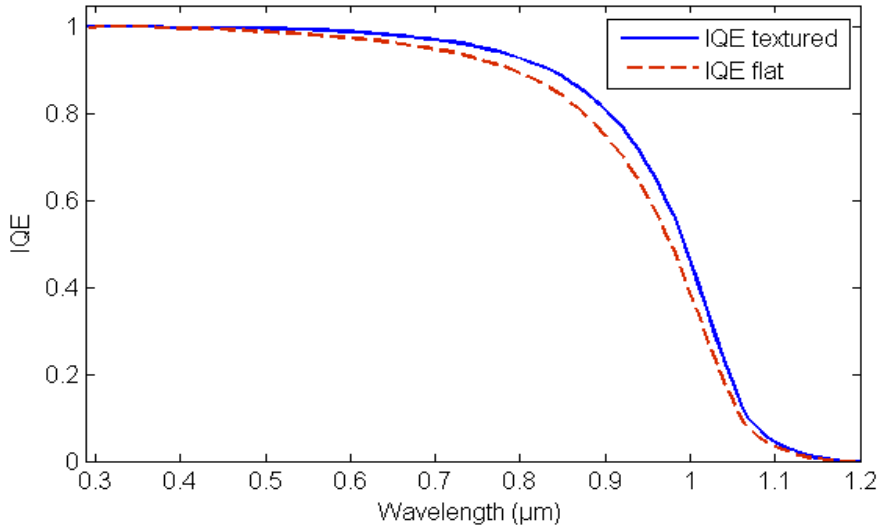


***Figure 5.6.*** *The IQE of a textured and flat silicon solar cell.*

From the graph it can be seen clearly that the IQE of a textured solar cell is higher in the longer wavelength region, i.e. when $\lambda > 0.8\ \mu m$. This is mainly due to the fact that surface textures result in enhanced path length of light providing low energy photons with higher absorption probabilities closer to the depletion region.

An even more obvious benefit of texturing silicon solar cells is seen from the following graph (Figure 5.7), where the EQE of a textured and flat silicon surfaces were calculated using equation 3.1 in Section 3.5.

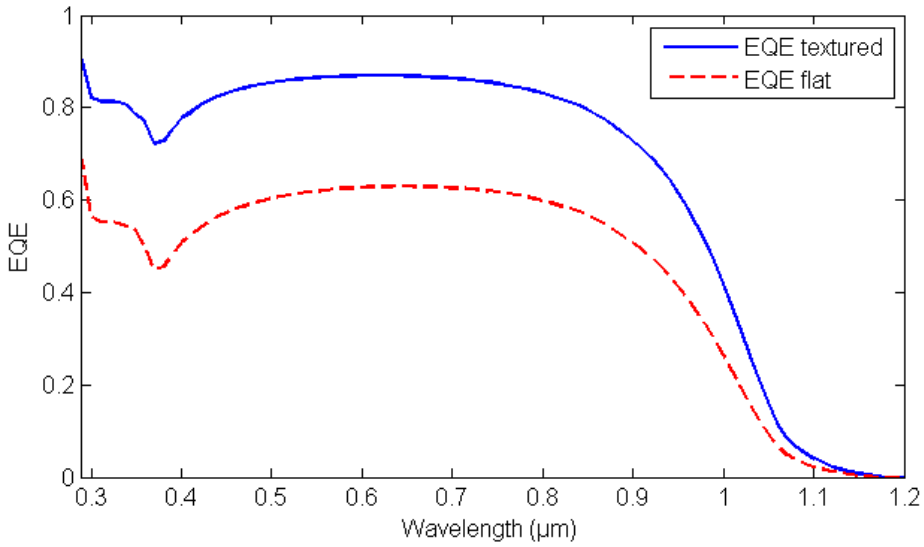


***Figure 5.7.*** *The EQE of a textured and a flat silicon solar cells.*

It can be seen that reduced front-face reflectance greatly increases the EQE of the cell. In the short wavelength range there seems to be a downward peak of the EQE values. A similar, yet positive, peak at the same wavelengths is seen in the reflectance values of different silicon surfaces (Figure 5.4), which is mainly due to the distribution of the refractive index of silicon. Essentially, if there is an increase in the reflectance value, there is a decrease in the EQE value.

## 5.4 Discussion

The analysis part of this thesis consists of two parts: modeling and calculating the reduced front-face reflectance of textured silicon cells, and analyzing the effect of textures on the overall solar cell performance through QE analysis.

The method chosen to analyze the reflectance of regular upright pyramids does not require the use of computationally intense and costly methods. Modeling surface textures with an analytical model provides resources to estimate the potential benefits of texturing prior to the production of a solar cell.

In the analysis, it was assumed that the etching technique appropriate to the silicon material and the etching parameters were optimal enough to create regular upright pyramids with high facet tilt angles of 54.74° yielding a double and triple bounce effects, that uniformly cover the silicon surface. The reflectance results obtained in the first part of the analysis were fairly consistent with the literature results. However, it must be emphasized that the obtained values of transmittance, especially at the third bounce, are slightly overestimated. Since the transmittance at the third bounce appears to be so low in the first place, especially in comparison with the transmittances of the first and second bounces, the error introduced when estimating the overall transmittance is not so large. As it was mentioned previously only 0.33 % of the initial incident light is transmitted at the third bounce. Nevertheless, in reality a smaller fraction of light is

transmitted, since the transmitted light beam at this bounce has a high probability of striking the opposite facet of the same pyramid. In addition, accounting for interference and diffraction effects would provide more accurate results; however, employing a geometrical optics regime would no longer be possible.

Analyzing front-face reflectance in solar cells provides us with the information of how much light was in fact able to penetrate the cell and thus potentially contribute to the cell's $J_{sc}$. It becomes clear that as the front-face reflectance decreases, the EQE of the cell significantly increases. However, it is also useful to investigate what happens with the IQE values of a textured cell in comparison with a perfectly smooth cell in order to assess other advantages/disadvantages of surface texturing in more depth.

In this thesis it was assumed that all light would be absorbed before reaching the back surface of a solar cell. A more sophisticated IQE analysis, in addition to other solar cell parameters, also includes the effects of internal front surface reflectance $\rho_{in}$, and in particular, back surface reflectance $\rho_{bs}$, since it plays an important role in determining the IQE of a cell at longer wavelengths, as it was pointed out in Chapter 3. On the other hand, due to the fact that $\rho_{bs}$ can be easily perfected and thus, its value can be set close to unity, when designing a silicon solar cell, neglecting $\rho_{bs}$ from the analysis can be justified.

The IQE analysis in this thesis does not provide much information on the deteriorating effect of increased surface area and thus, increased front surface recombination velocity in textured solar cells. This is because the contributions of the emitter and the space charge regions when estimating the IQE of a textured and flat silicon solar cell were ignored. Therefore, in Figure 5.6 at short wavelengths ($\lambda < 0.5\ \mu m$) there seems to be no difference between the IQE values of textured and flat solar cells. The IQE of a flat cell, in reality, is expected to be slightly higher than the IQE of a textured cell at such wavelengths. However, as it was pointed out in Section 3.5, the beneficial influence of the path length enhancement due to texturing surpasses the detrimental effect of increased surface recombination velocity. Furthermore, as mentioned, an increase in front surface recombination would only affect a small fraction of the wavelength range of interest. However, more accurate results could have been provided if the contributions of the space charge region and especially the emitter region and thus, the surface recombination velocities, were taken into account. Such simplification also implies that this analysis is limited to thick silicon solar cells. As mentioned, when analyzing the IQE of thin films considering the contributions to the IQE of all cell regions is particularly important.

## 5.5 Future development

In this thesis, reflectance and transmittance analyses were performed only a certain type of texture: the regular upright pyramids. A subject for further investigation could be, for instance, determining whether other surface morphologies provide significant enhancement in the overall cell transmittance and short-circuit current.

In this thesis only the FFT was examined. As mentioned, light trapping schemes can be performed by incorporating pyramidal structures on both top and back surfaces. Another subject for future work would be to investigate how texturing both front and back surfaces of the cell would affect the cell's QE. However, it must be taken into account that texturing the back surface would also involve multiple bounces of light on the rear reflector and would reduce the back surface reflectance and hence the internal quantum efficiency at longer wavelengths.

The IQE results seem to be greatly dependent on the absorption coefficient of the silicon material. Therefore, accurately determining this coefficient is crucial in the analysis. The absorption coefficient values used in this analysis were determined at 300 K (Green, 2008). An indication of conversion efficiency and parameter extraction (diffusion length and recombination velocities), both provided by IQE analysis, are important under varying operating conditions. The temperature of an individual cell can vary from 258 to 353 K. Thus, in order to provide a more comprehensive analysis, the variation of absorption coefficient with temperature and its influence on the solar cell performance can be investigated.

The investigation of texturing and its influence on solar device performance can be extended to other solar cells rather than just silicon solar cells. For instance, the influences of reduced front-face reflectance on solar cell performance can be investigated in organic solar cells and thin films cells. It can be researched, which types of textures are available for other solar cell materials, what their dimensions are, and whether or not creating these textures is cost-effective.

# 6 CONCLUSION

Silicon is one of the most commonly used semiconductor material in solar cell applications. The main reasons for that is the fact that silicon's absorption characteristics match fairly well the solar spectrum and the fabrication technology of silicon is well developed. However, silicon tends to have very high surface reflectance: approximately 30-40% of incident light is reflected from the bare silicon surface. Creating surface textures is one effective method to significantly reduce front-face reflectance. This is due to the ability of textures to scatter incident light and enhance light trapping within the cell.

The aim of this thesis was to investigate which types of surface textures are available for silicon solar cells and what are their impacts on such devices. It was of particular interest what kind of surface morphologies and dimensions these textures include. A brief literature review showed that state-of-the-art texturing techniques consist of different types of etching approaches. The etching technique and the results produced greatly depend on whether the silicon surface material used is monocrystalline or multicrystalline. Alkaline etching is used to produce pyramidal structures on (100) oriented monocrystalline silicon solar cell surface. Alkaline etching has an anisotropic nature, which causes etching to occur more readily in a particular crystallographic orientation in silicon than in another. Therefore, as an end result, the textured surfaces become composed of slow etching planes. Exposing (100) orientated planes to such etching techniques reveals intersections of (111) facets, thus creating a pyramidal morphology. With the optimal etching time and other procedure parameters, the pyramids created have a common feature of a high facet-tilt angle, which guarantees improved front surface antireflection properties, as well as uniform surface coverage. Acidic (isotropic) etching and reactive-ion etching are more suitable techniques for multicrystalline silicon revealing other surface morphologies besides pyramids as well, such as periodic grooves. It was, nevertheless, observed that texturing multicrystalline silicon yields poorer reflectance results than texturing monocrystalline silicon. The literature review also revealed that inverted regular pyramid structures provide the best optical enhancements. Surface texture characteristics, such as dimensions and coverage are essential when modeling light behavior on such surfaces.

In this thesis, various types of modeling of textured surfaces were investigated. The investigation revealed that modeling textured surfaces include two main approaches; the geometrical optics and physical optics regime. An analytical model based on geometrical optics was used to examine the optical behavior of a solar cell with a textured front surface. Analytical models of such problems, including the chosen analytical

model, are somewhat simplified. However, the comparison of reflectance value of ~10% obtained in the wavelength range of 0.29-1.195 μm seemed to be consistent with the results found in other studies, where reflectance was either measured or calculated. The obtained value of reflectance was significantly lower than the reflectance values of bare silicon and silicon surface with a $SiO_2$ antireflection coating of an optimal thickness. The simulation results also showed that such a complex problem as modeling light behavior on textured surface can be well-approximated by an analytical model. Nevertheless, in order to obtain more accurate results, numerical analysis, such as ray tracing or finite-element methods that rigorously solves Maxwell equations, are required.

In the reflection analysis it was assumed that the structures, which were regular upright pyramids, had a high facet tilt angle (54.74°) and a uniform coverage. Such textures have higher chances of being formed on monocrystalline silicon surface through alkaline etching with optimal etching parameters, such as time, temperature and solution concentration. As mentioned, despite a fairly good accuracy of the obtained reflectance result, the overall results were nevertheless, an approximation of the real value due to some simplifications implied when solving a complex problem of such kind analytically. For instance, light was considered to travel directly into the bulk at the second and third bounces, which slightly overestimates the transmittance result. However, considering the resources and time it takes to perform a full numerical analysis, this is a fairly good approximation and depending on the nature of the study can provide sufficient accuracy.

Finally, the IQE of a textured solar cell and a flat solar cell were analyzed. By calculating the quantum efficiency of a cell, the contributions to the short-circuit current of different wavelengths can be determined. It is therefore very practical to calculate the QE when attempting to improve the conversion efficiency of a cell. The most benefits of surface textures can be seen in the EQE results, where the EQE values of a textured solar are significantly higher than the EQE values of a flat cell. However, the analysis and results found in the literature revealed that surface textures also provide an increase in the longer wavelength region, particularly when $\lambda > 0.8\,\mu m$. This is because the normally incident light beam is tilted at the surface texture and thus travels a longer path having more chances to absorbed, as well as having more chances to be absorbed closer to the depletion region.

IQE analysis aims at determining the diffusion lengths of different regions, as well as the surface recombination velocities. In this thesis, only FFT configuration was assumed, therefore the back surface recombination velocity was considered to not be influenced by textures. In addition, the solar cells, flat and textured, were assumed to be large enough to absorb all the light before it reaches the back surface. Naturally, with such simplification, both back surface recombination velocity and back surface reflectance do not play a role in determining the IQE of a cell. It was also shown in other studies that back surface recombination velocity has little impact on the cells' IQE in general. Many studies showed that the back surface reflectance proved however, to affect the IQE.

Since, the total IQEs of both cells were approximated by the IQE of the base region, front surface recombination velocity did not affect the results derived in this analysis. This assumption was justified due to the fact, that studies have shown that the total IQE of the cell portrays little dependence on the front surface recombination, especially in comparison with other parameters, such as the base diffusion length, and is mostly affected at short wavelengths, when $\lambda < 0.5\ \mu m$. However, considering all the assumptions made in this thesis, it must be highlighted that the validity of the results is restricted only to very thick silicon solar cells.

To conclude, it becomes obvious that texturing solar cell significantly decreases the front-face reflectance and thus, improves the EQE, as well as the IQE of the cell. The detrimental effect to the cell's electrical properties due to an increase in surface area is insignificant in thick silicon solar cells and can be resolved by passivating the emitter surface.

# REFERENCES

Aberle, A. G. 2000. Surface passivation of crystalline silicon solar cells: a review. Progress in Photovoltaics: Research and Applications 8, 5, pp. 473-487.

Arvo, J., Dutre, P., Keller, A., Jensen, H. W., Owen, A., Pharr, M. & Shirley, P. 2003. Monte Carlo ray tracing. San Diego, University of California. 171p.

Baker-Finch, S. C. & McIntosh, K. R. 2010. Reflection of normally incident light from silicon solar cells with pyramidal texture. Progress in Photovoltaics: Research and Applications 19, 4, pp. 406-416.

Basore, P. A. 1990. Numerical modeling of textured silicon solar cells using PC-1D. Electron Devices 37, 2, pp. 337-343.

Bean, K. E. (1978). Anisotropic etching of silicon. IEEE Transactions on Electron Devices 25, 10, pp. 1185-1193.

Blakers, A. W., Wang, A., Milne, A. M., Zhao, J. & Green, M. A. (1989). 22.8% efficient silicon solar cell. Applied Physics Letter 55, 13, pp. 1363-1365.

Brendel, R., Hirsch, M., Plieninger, R. & Werner, J. J. 1996. Quantum efficiency analysis of thin-layer silicon solar cells with back surface fields and optical confinement. Electron Devices 43, 7, pp. 1104-1113.

Bressers, P. M., Kelly, J. J., Gardeniers, J. G. & Elwenspoek, M. (1996). Surface Morphology of p-Type (100) Silicon Etched in Aqueous Alkaline Solution. Journal of the Electrochemical Society 143, 5, pp. 1744-1750.

Bücher, K., Bruns, J. & Wagemann, H. G. (1994). Absorption coefficient of silicon: An assessment of measurments and the simulation of temperature variation. Journal of Applied Physics 75, 2, pp. 1127-1132.

Byun, S.-J., Buyn, S. Y., Lee, S. Y., Kim, J. W., Cho, K., Sheen, D., Tark, S. J., Kim, D. & Kim, W. M. 2011. Analysis of light trapping effects in Si solar cells with a textured surface by ray tracing simulation. Current Applied Physics 11, 4, pp. S23-S25.

Campbell, P. 1993. Enhancement of light absorption from randomizing and geometric textures. Journal of the Optical Society of America B 10, 12, pp. 2410-2415.

Chen, F. & Wang, L. 2011. Light Trapping Design in Silicon-Based Solar Cells. InTech, Wuhan University of Technology. 364 p.

Clugston, D. A. & Basore, P. A. 1997. PC-1D version 5: 32-bit solar cell modeling on personal computers. Photovoltaic Specialists Conference, Anaheim, California, USA September 29-October 03, 1997, pp. 207-210.

De Wolf, S., Choulat, P., Vazsonyi, E., Einhaus, R., Van Kerschaver, E., De Clercq, K. & Szlufcik, J. 2000. Towards industrial application of isotropic texturing for multi-crystalline silicon solar cells. Proceedings of the 16th European Photovoltaic Solar Energy Conference, Glasgow, UK, 2000, pp. 1521-1523.

Dell, R. M. & Rand, D. A. 2004. Clean Energy. Cambridge, Royal Society of Chemistry. 383 p.

DiStefano, T. H. 2009. Reduction of grain boundary recombination in polycrystalline silicon solar cells. Applied Physics Letters 30, 7, pp. 351-353.

Fonash, S. J. 2010. Solar Cell Device Physics. 2 ed. Burlington, Academic Press. 381 p.

Fraas, L. & Partain, L. 2010. Solar Cells and Their Applications. 2 ed. Hoboken, New Jersey, John Wiley & Sons. 648 p.

Fukui, K., Inomata, Y. & Shirasawa, K. 1997. Surface texturing using reactive ion etching for multicrystalline silicon solar cell. Proceedings of the 26th IEEE Photovoltaic Specialists Conference, Anaheim, California, USA, September 29-October 03, 1997, pp. 47-50.

Gjessing, J. 2012. Photonic crystals for light trapping in solar cells. Dissertation. Oslo, Norway. University of Oslo, Faculty of Mathematics and Natural Sciences, No. 1163. 164 p.

Green, M. A. 1987. High Efficiency Silicon Solar Cells. Aedermannsdorf, Switzerland, Trans Tech Publications. 240 p.

Green, M. A. 1999. High-efficiency silicon solar cells. Switzerland. Electronics and Structures for MEMS, Trans. Tech. Publications.

Green, M. A. 2008. Self-consistent optical parameters of intrinsic silicon at 300 K including temperature coefficients. Solar Energy Materials and Solar Cells 92, 11, pp. 1305-1310.

Green, M. A., Emery, K., Hishikawa, Y., Warta, W., & Dunlop, E. D. 2012. Solar cell efficiency tables (version 39). Progress in Photovoltaics: Research and Applications 20, 1, pp. 12-20.

He, X. D., Torrance, K. E., Sillion, F. X. & Greenberg, D. P. 1991. A comprehensive physical model for light reflection. Computer Graphics 25, 4, pp. 175-186.

Honsberg, C. B. 2012. Photovoltaic Education Network [WWW]. [Cited 15/07/2013] Available at: http://www.pveducation.org/pvcdrom.

Hylton, J. D. 2006. Light coupling and light trapping in alkaline etched multicrystalline silicon wafers for solar cells. Dissertation. Utrecht, Netherlands. Utrecht University. Faculty of Science. 182 p.

Hylton, J. D., Burgers, A. R. & Sinke, W. C. 2004. Alkaline etching for reflectance reduction in multicrystalline silicon solar cells. Journal of Electrochemical Society 151, pp. G408-G427.

Jha, A. R. 2010. Solar Cell Technology and Applications. Boca Raton, Taylor and Francis Group. 304 p.

Luque, A. & Hegedus, S. 2010. Handbook of Photovoltaic Science and Engineering. 2 ed. West Sussex, John Wiley & Sons. 1162 p.

Macdonald, D. H., Cuevas, A., Kerr, M. J., Samundsett, C., Ruby, D., Winderbaum, S. & Leo, A. 2004. Texturing industrial multicrystalline silicon solar cells. Solar Energy 76, 1-3, pp. 277-283.

Markvart, T. & Castaner, L. 2004. Solar Cells: Materials, Manufacture and Operation. Oxford, Elsevier. 600 p.

Meng, F. Y. 2001. Grain boundary theory and photovoltaic characteristics of solar cell on polycrystalline silicon material. Dissertation. Shanghai, China. Shanghai Jiaotong University.

Miles, R. W., Hynes, K. M. & Forbes, I. 2005. Photovoltaic solar cells: An overview of state-of-the-art cell development and environmental issues. Progress in Crystal Growth and Characterization of Materials 51, 1-3, pp. 1-42.

Möller, H. J., Funke, C., Rinio, M. & Scholz, S. 2005. Multicrystalline silicon for solar cells. Thin Solid Films 478, 1-2, pp. 179-187.

Nishimoto, Y., Ishihara, T. & Namba, K. 1999. Investigation of Acidic Texturization for Multicrystalline Silicon Solar Cells. Journal of the Electrochemical Society 146, 2, pp. 457-461.

Panek, P., Lipiski, M. & Dutkiewicz, J. 2005. Texturization of multicrystalline silicon by wet chemical etching for silicon solar cells. Journal of Materials Science 40, 6, pp. 1459-1463.

Poruba, A., Fejfar, A., Remeš, Z., Špringer, J., Vaněček, M., Kočka, J., Meier, J. Torres, P. & Shah, A. 2000. Optical absorption and light scattering in multicrystalline silicon thin films and solar cells. Journal of Applied Physics 8, 88, pp. 148-160.

Polyanskiy, M. 2013. Refractive index database [WWW]. [Cited 16/07/2013]. Available at: http://refractiveindex.info/?group=CRYSTALS&material=SiO2

Reynolds, J. H. & Meulenberg, A. 1974. Measurment of diffusion length in solar cells. Journal of Applied Physics 45, 6, pp. 2583-2592.

Rodriguez, J. M., Tobias, I. & Luque, A. 1997. Random pyramidal texture modelling. Energy and Solar Cells 45, 3, pp. 241-253.

Ruby, D., Zaidi, S., Roy, M. & Narayanan, M. 1999. Plasma texturing of silicon solar cells. Proceedings of the 9th Workshop on the Role of Impurities and Defects in Silicon Device Processing. Colorado, USA. 1999. pp. 179-182.

Siegel, R. & Howell, J. 2002. Thermal radiation heat transfer. 5 ed. New York, Taylor and Francis. 987 p.

Singh, P. K., Kumar, R., Lal, M., Singh, S. N. & Das, B. K. 2001. Effectiveness of anisotropic etching of silicon in aqueous alkaline solutions. Solar Energy Materials and Solar Cells 70, 1, pp. 103-113.

Sinton, R. A. & Cuevas, A. 1996. Contactless determination of current–voltage characteristics and minority-carrier lifetimes in semiconductors from quasi-steady-state photoconductance data. Applied Physics Letters 69, 17 pp. 2510-2512.

Sinton, R. A., Kwark, Y., Gan, J. Y. & Swanson, R. M. 1986. 27.5-Percent Silicon Concentrator Solar Cells. Electron Device Letters, IEEE 7, 10, pp. 567-569.

Smith, A. W. & Rohatgi, A. 1993. Ray tracing analysis of the inverted pyramid texturing geometry for high efficiency silicon solar cells. Solar Energy Materials and Solar Cells , 29, pp. 37-49.

Stephens, B. R. & Cody, G. D. 1977. Optical reflectance and transmission of a textured surface. Thin Solid Films 45, 1, pp. 19-29.

Terman, L. M. 1961. Spectral response of solar-cell structures. Solid-State Electronics 2, 1, pp. 1-7.

Tiedje, T., Yablonovitvh, E., Cody, G. D. & Brooks, B. G. 1984. Limiting Efficiency of Silicon Solar Cells. IEEE Transactions on Electron Devices 31, 5, pp. 711-716.

Torrance, K. E. & Sparrow, E. M. 1967. Theory for Off-Specular Reflection From Roughned Surfaces. Journal of Optical Society of America 57, 9, pp. 1105-1112.

Trupke, T., Daub, E. & Wurfel, P. 1997. Absorptivity of silicon soalr cells obtained from luminescence. Solar Energy Materials and Solar Cells 53, 1-2, pp. 103-114.

Verlinde, P., Evrard, O., Mazy, E. & Crahay, A. 1992. The surface texturization of solar cells: A new method using V-grooves with controllable sidewall angles. Solar Energy Materials and Solar Cells 26, 1-2, pp. 71-78.

Wang, A., Zhao, J. & Green, M. A. 1990. 24% efficient silicon solar cells. Applied Physics Letters 57, 6, pp. 602-604.

Winderbaum, S., Reinhold, O. & Yun, F. 1997. Reactive ion etching (RIE) as a method for texturing polycrystalline silicon solar cells. Solar Energy Materials and Solar Cells 48, 3, pp. 239-248.

Xi, Z., Yang, D., Dan, W., Jun, C., Li, X. & Que, D. 2004. Investigation of texturization for monocrystalline silicon solar cells with different kinds of alkaline. Renewable Energy 29, 13, pp. 2101-2107.

Yagi, T., Uraoka, Y. & Fuyuki, T. 2006. Ray-trace simulation of light trapping in silicon solar cell with texture structures. Solar Energy Materials and Solar Cells 90, 16, pp. 2647-2656.

Yang, W. J., Ma, Z. Q., Tang, X., Feng, C. B., Zhao, P. P. & Shi, P. P. 2008. Internal quantum efficiency for solar cells. Solar Energy 82, 2, pp. 106-110.

Young, H. & Freedman, R. 2008. University physics with modern physics. 12 ed. San Francisco, Pearson Addison-Wesley. 1632 p.

Zeghbroeck, B. 2004. Principles of semiconductor devices [WWW]. [Cited 02/07/2013]. Available at: http://ecee.colorado.edu/~bart/book/

Zhao, J. & Green, M. A. 1991. Optimized antireflection coatings for high-efficiency silicon solar cells. Electron Devices 38, 8, pp. 1925-1934.

# APPENDIX: SIMULATION CODE

```
x=[all given values] %Wavelength range, an array of values (average of
each interval)

n1=1 %Refractive index of air

n2=[all given values that correspond to each x]

I=[all given values that correspond to each x]


%Function to calculate reflectance directly for each bounce --> first
bounce. %Can be called by ReflectanceDirect1(n1,n2)
function[rho]=ReflectanceDirect1(n1,n2)
theta=degtorad(54.74);
theta2=asin((n1./n2)*sin(theta)); %Snell's law to calculate the trans-
mitted angle

% n2 is an array, theta2 is an array, r_s and r_p are arrays, rho_s
and
% rho_p are arrays; and finally the answer rho should be an array
%plot(x, ReflectanceDirect1(n1, n2)

r_s=-(n2.*cos(theta2)-
n1.*cos(theta))./((n2.*cos(theta2))+n1.*cos(theta));
r_p=(n2.*cos(theta)-
n1.*cos(theta2))./(n2.*cos(theta)+n1.*cos(theta2));
rho_s=r_s.^2;
rho_p=r_p.^2;
rho=(rho_s+rho_p)/2;
end

%Function to calculate reflectance directly for each bounce --> second
bounce. Can be called by ReflectanceDirect2(n1,n2)
function[rho]=ReflectanceDirect2(n1,n2)
theta=degtorad(15.79);
theta2=asin((n1./n2)*sin(theta)); %Snell's law to calculate the trans-
mitted angle

r_s=-(n2.*cos(theta2)-
n1.*cos(theta))./((n2.*cos(theta2))+n1.*cos(theta));
r_p=(n2.*cos(theta)-
n1.*cos(theta2))./(n2.*cos(theta)+n1.*cos(theta2));
rho_s=r_s.^2;
rho_p=r_p.^2;
rho=(rho_s+rho_p)/2;
```

```
end

%Function to calculate reflectance directly for each bounce --> third
bounce. Can be called by ReflectanceDirect3(n1, n2)
function[rho]=ReflectanceDirect3(n1,n2)
theta=degtorad(86.39);
theta2=asin((n1./n2)*sin(theta)); %Snell's law to calculate the trans-
mitted angle

r_s=-(n2.*cos(theta2)-
n1.*cos(theta))./((n2.*cos(theta2))+n1.*cos(theta));
r_p=(n2.*cos(theta)-
n1.*cos(theta2))./(n2.*cos(theta)+n1.*cos(theta2));
rho_s=r_s.^2;
rho_p=r_p.^2;
rho=(rho_s+rho_p)/2;
end


%TRANSMITTED FLUX

%Function returns the total transmitted fraction of light from the
regular upright pyramidal structure from path A and path B

function[I_T]=TransmittedFlux(I, rho1, rho2, rho3)
%Function returns the total reflected fraction of light from the regu-
lar upright pyramidal structure from path A and path B



%Calculating the refracted angles at each bounce in global coordinates

%The function can be called: TransmittedFlux(I,
%ReflectanceDirect1(n1,      n2),      ReflectanceDirect2(n1,      n2),
ReflectanceDirect3(n1, n2))
%n2=[all values]
%similarly x=[all values]

T_1a=(1-rho1).*I; %Transmitted flux at the first bounce from path A
T_2a=(1-rho2).*rho1.*I;  %Transmitted  flux  at  the  second  and  final
bounce from path A

T_1b=(1-rho1).*I; %Transmitted flux at the first bounce from path B
T_2b=(1-rho2).*rho1.*I;  %Transmitted  flux  at  the  second  bounce  from
path B
T_3b=(1-rho3).*rho2.*rho1.*I; %Transmitted flux at the third and final
bounce from path B
```

```
I_ta=T_1a + T_2a; %Transmitted flux from path A; a sum of two trans-
mitted fluxes

I_tb= T_1b + T_2b + T_3b; %Transmitted flux from path B; a sum of
three transmitted fluxes

%Total transmitted flux as a sum of weighted transmitted fluxes from
path A and path B.

I_T=0.8889*I_ta+0.1111*I_tb;
    end

%REFLECTED FLUX

%Function returns the total reflected fraction of light from the regu-
lar upright pyramidal structure from path A and path B

%REFLECTED FLUX

%Function returns the total reflected fraction of light from the regu-
lar upright pyramidal structure from path A and path B

function [I_R]=ReflectedFlux(I, rho1, rho2, rho3)

%Function can be called as: ReflectedFlux(I,
%ReflectanceDirect1(n1,      n2),      ReflectanceDirect2(n1,      n2),
ReflectanceDirect3(n1, n2))

%Calculating the refracted angles at each bounce in global coordinates

I_ra=rho2.*rho1.*I; %Reflected flux for path A
I_rb=rho3.*rho2.*rho1.*I; %Reflected flux for path B

%Total reflected flux as a sum of weighted reflected fluxes from path
A and path B

I_R=0.8889.*I_ra+0.1111.*I_rb;

    end


%Function to calculate the reflectance of a completely flat surface.
Can be called as
%ReflectanceFlatSurface(n1,n2)
function[rho]=ReflectanceFlatSurface(n1,n2)
theta=degtorad(0); %Normally incident light
theta2=asin((n1./n2)*sin(theta)); %angle of refraction
%Naturally the transmitted angle is already in global coordinates
```

```
%Transmittance and reflectance must also be as angular distribution


% rho_p are arrays; and finally the answer rho should be an array

r_s=-(n2.*cos(theta2)-
n1.*cos(theta))./((n2.*cos(theta2))+n1.*cos(theta));  %Fresnel  coeffi-
cient of perpendicularly polarized light
r_p=(n2.*cos(theta)-
n1.*cos(theta2))./(n2.*cos(theta)+n1.*cos(theta2));  %Fresnel  coeffi-
cient of parallel polarized light
rho_s=r_s.^2; %reflectance of s-polarized light
rho_p=r_p.^2; %reflectance of p-polarized light
rho=(rho_s+rho_p)/2; %reflectance of non-polarized light
end

function [I_R]=ReflectedFluxFlatSurface(rho, I)
%Reflected    flux    for    each    path.    To    call    function
ReflectedFluxFlatSurface(ReflictivityFlatSurface(n1, n2), I)

%Total reflected flux

I_R=rho.*I;

%Angular distribution needs to be added

    end

function [theta1tgd]=TransmittedAngleGlobalFirstBounce(n1, n2)
%First bounce:

theta1=degtorad(54.74); %Incident angle of the first bounce
theta1t=asin((n1./n2)*sin(theta1)); %Refracted  angle  in  local  coordi-
nates
theta1tg=theta1-theta1t; %Refracted angle in global coordinates
theta1tgd=radtodeg(theta1tg);
end


function [theta2tgd]=TransmittedAngleGlobalSecondBounce(n1, n2)
%Second bounce:
theta1=degtorad(54.74);
theta2=degtorad(15.79); %Incident angle of the second bounce
theta2t=asin((n1./n2)*sin(theta2)); %Refracted  angle  in  local  coordi-
nates
theta2tg=theta1+theta2t; %Refracted angle in global coordinates
theta2tgd=radtodeg(theta2tg);
end
```

```
function [theta3tg]=TransmittedAngleGlobalThirdBounce(n1, n2)

function [theta3tgd]=TransmittedAngleGlobalThirdBounce(n1, n2)

%Third bounce:
theta1=degtorad(54.74);
theta3=degtorad(86.39); %Incident angle of the third bounce
theta3t=asin((n1./n2)*sin(theta3)); %Refracted angle in local coordi-
nates
theta3tg=theta1+theta3t; %Refracted angle in global coordinates
theta3tgd=radtodeg(theta3tg);
end

function[T_1a]=TransmittanceFirst(rho1)
%Transmittance at the first bounce of path A and B
%Function can be called as
TransmittanceFirst(ReflectanceDirect1(n1,n2))
T_1a=(1-rho1);
end

function[T_2a]=TransmittanceSecond(rho1, rho2)
%Transmittance at the second bounce of path A and B
%Function can be called as
TransmittanceSecond(ReflectanceDirect1(n1,n2),ReflectanceDirect2(n1,n2
))
T_2a=(1-rho2).*rho1;
end

function[T_3b]=TransmittanceThird(rho1, rho2, rho3)
%Transmittance at the third bounce of path B
%Function can be called as
TransmittanceThird(ReflectanceDirect1(n1,n2),ReflectanceDirect2(n1,n2)
, ReflectanceDirect3(n1,n2))
T_3b=(1-rho3).*rho2.*rho1;
end


function[R]=ReflectanceARC(x, n1, n2)

%A function that calculates the reflectance of an ARC
n0=sqrt(1.28604141+(1.07044083*x.^2)./(x.^2-
0.0100585997)+(1.10202242*x.^2)./(x.^2-100)); %Determines the refrac-
tive index of SiO2 coating

d=x./4*n1; %Optimal thickness of the ARC

%Reflectance at normal incidence, parameters:
r1=(n1-n0)./(n1+n0);
```

```
r2=(n0-n2)./(n0+n2);
theta=2*pi*n0.*d./x;

%Reflectance of angle layer of SiO2 on a substrate

R=((r1.^2)+(r2.^2)+2*r1.*r2.*cos(2*theta))./(1+(r1.^2).*(r2.^2)+2*r1.*
r2.*cos(2*theta));
     end
```